Title: **Anatexis and fluid regime of the deep continental crust: new clues from melt and fluid inclusions in metapelitic migmatites from Ivrea Zone (NW Italy)**

Short running title: **Anatexis and fluid regime: clues from melt inclusions**

Authors: Carvalho, Bruna B.[1,*], Bartoli, Omar[1], Ferri, Fabio[1], Cesare, Bernardo[1], Ferrero, Silvio[2,3], Remusat, Laurent[4], Capizzi, Luca[1,5], Poli, Stefano[5]

Affiliations:

[1]*Dipartimento di Geoscienze, Università degli Studi di Padova, Via G. Gradenigo, 6, 35131, Padova, Italy.*

[2]*Institut für Erd- und Umweltwissenschaften, Universität Potsdam, 14476, Potsdam, Germany.*

[3]*Museum für Naturkunde (MfN), Leibniz-Institut für Evolutions- und Biodiversitätsforschung, 10115, Berlin, Germany.*

[4]*Muséum National d'Histoire Naturelle, Sorbonne Université, UMR CNRS 7590,lRD, lnstitut de Minératogie, de Physique des Matériaux et de Cosmochimie, IMPMC, 75005 Paris, France.*

[5]*Dipartimento di Scienze della Terra, Università degli Studi di Milano, via Mangiagalli 34, 20133, Milan, Italy.*

*Corresponding author: bruna.borgescarvalho@unipd.it

ABSTRACT

We investigate the inclusions hosted in peritectic garnet from metapelitic migmatites of the Kinzigite Formation (Ivrea Zone, NW Italy) to evaluate the starting composition of the anatectic melt and fluid regime during anatexis throughout the upper amphibolite-facies, transitional and granulite-facies zones. Inclusions have negative crystal shapes, size from 2 to10 μm and are regularly distributed in the core of the garnet. Microstructural and micro-Raman investigations have shown the presence of two types of inclusions: crystallized silicate melt inclusions (i.e. nanogranitoids, hereafter NI) and fluid inclusions (FI). Microstructural evidence suggests that FI and NI coexist in the same cluster and are primary (i.e. were trapped simultaneously during garnet growth). FI have similar composition in the three zones and comprise variable proportions of CO_2, CH_4 and N_2, commonly with siderite, pyrophyllite and kaolinite. The mineral assemblage in the NI contains K-feldspar, plagioclase, quartz, biotite, muscovite, chlorite, graphite and, sometimes, calcite. Polymorphs such as kumdykolite, cristobalite and tridymite were also found.

Re-homogenized NI from the different zones and show that all the melts are leucogranitic but have slightly different compositions. In samples from the upper amphibolite facies, melts are less mafic (FeO+MgO 2- 3.4 wt. %), contain 860-1700 ppm CO_2 and reach the highest H_2O contents (6.5-10 wt. %). In the transition zone melts have intermediate H_2O (4.8-8.5 wt. %), CO_2 (457-1534 ppm) and maficity (FeO+MgO 2.3- 3.9 wt. %). In contrast, melts at granulite facies reach highest CaO, FeO+MgO (3.2-4.7 wt. %) and CO_2 (up to 2400 ppm), with H_2O contents comparable (5.4-8.3 wt. %) to the other two zones.

Our data suggests that anatexis of these metapelites occurred through muscovite and biotite breakdown melting in the presence of a COH fluid. The fluid is assumed to be internally derived, produced initially by devolatilization of hydrous silicates in the graphitic protolith, then as result of oxidation of carbon by melting of Fe^{3+}-bearing biotite. Variation in the composition of the melts are interpreted to result from combination of higher T of melting, greater contribution of anhydrous reactants (such as plagioclase) and minor role of apatite. The H_2O contents of the melts throughout the three zones are comparable and higher than usually assumed. While the CO_2 contents are highest at

granulite facies, and show that carbon-contents of crustal magmas may not be completely negligible. The a_{H2O} of the fluid dissolved in granitic melts decreases with increasing metamorphic grade.

Key words: melt inclusions, fluid inclusions, anatexis, CO_2-H_2O contents of melts, Ivrea Zone.

1. INTRODUCTION

The rise of temperature during metamorphism occurs in response to tectonic processes that build orogenic and collisional mountain belts of the Earth, or that extend the lithosphere during continental rifting. In particular, the high- (HT) to ultrahigh-temperature (UHT) metamorphism may lead to partial melting of the middle and lower crust. Anatexis, subsequent segregation and transfer of the crustal melt to the upper crust are the mechanisms that control crustal differentiation (e.g. Vielzeuf, Clemens, Pin, & Moinet, 1990; Sawyer, Cesare, & Brown, 2011; Brown, 2013). As a result, the continental crust has become progressively stratified throughout Earth's history, with a more residual and mafic lower crust, enriched in elements such as FeO, MgO, Al_2O_3, CaO and a more silicic upper crust, enriched in K_2O, SiO_2 and incompatible trace elements.

Migmatites and granulites are widespread in the deep crust and, once at the surface, provide fundamental information on how crustal magmas are generated. However, the investigation of melt rich-rocks (i.e. leucosomes, diatexites) is not a straightforward way to access the starting compositions of the melts, especially in terms of volatiles. The main reason is because there are several processes happening simultaneously at the source that modify the melt compositions; for instance, crystal fractionation (e.g., Sawyer, 1987; Milord, Sawyer, & Brown, 2001; Brown et al., 2016; Carvalho, Sawyer, & Janasi, 2016), restite unmixing (Chappell, White, & Wyborn, 1987), entrainment of peritectic or residual phases (Stevens, Villaros, & Moyen, 2007; Clemens & Stevens, 2012; Sawyer, 2014), entrainment of less fertile lithologies (Carvalho, Sawyer, & Janasi, 2017) and volatile exsolution and diffusion (White & Powell, 2010).

An alternative, but very robust, way to recover the initial composition of the melts is to use melt inclusions (MI) or nanogranitoid inclusions (NI) found in peritectic minerals (Cesare, Ferrero, Salvioli-Mariani, Pedron, & Cavallo, 2009; Cesare, Acosta-Vigil, Bartoli, & Ferrero, 2015, Bartoli, Acosta-Vigil, Ferrero, & Cesare, 2016; Ferrero & Angel, 2018). Peritectic minerals form as result of incongruent melting reactions, and in some cases, they can trap droplets of the coexisting anatectic melt (Cesare et al., 2015) and of the fluid immiscible with it, if present (e.g. Ferrero, Braga, Berkesi, Cesare, & Laridhi, 2014; Tacchetto et al., 2018). These droplets of melt can be preserved as tiny (2-10 μm) glassy or crystallized (i.e. nanogranitoid) inclusions and they are the best way to investigate the in situ starting composition of the melt and fluid regime during crustal melting (e.g. Bartoli et al., 2013a; Bartoli, Acosta-Vigil, Ferrero, & Cesare, 2016).

In the latest years, the MI and NI have become fundamental tools to investigate crustal petrology and geochemistry. Despite of their small size, which poses analytical challenges, these inclusions have helped to unravel the anatectic history of polymetamorphic terranes (Acosta-Vigil et al., 2016), fluid regime of high grade terranes and initial volatile contents of granitic magmas (Bartoli, Cesare, Remusat, Acosta-Vigil, & Poli, 2014; Ferrero, Wunder, Walczak, O'Brien, & Ziemann, 2015; Bartoli et al., 2016). Composition of MI can also be useful to evaluate melt loss and reconstruct the prograde history of granulite terranes (Bartoli, 2017; 2018).

The Ivrea Zone, NW Italy, is a world-renowned section of mid to lower Permian continental crust where the preserved field gradient offers the opportunity to examine the evolution of crustal melting in nature. In this contribution, we describe for the first time the coexistence of primary melt and fluid inclusions in garnet from metapelitic migmatites of Val Strona di Omegna and use them to investigate crustal anatexis of this high-grade terrane from upper amphibolite to granulite facies, thereby contributing to better understand the processes that lead to crustal differentiation. The main points addressed are: (i) compositions of the melts ii) their evolution with increasing metamorphic grade, (iii) their implications for fluid regime of this high grade terrane.

2. GEOLOGICAL SETTINGS

The Ivrea Zone (IZ, NW Italy) is a section of the mid to lower Permian continental crust which comprises very well-preserved high-grade rocks (Schmid & Wood, 1976), and is limited by the Insubric line at the west and by the Cossato-Mergozzo-Brissago Line at east (Fig. 1a).

Two main units are recognized in the IZ, the Mafic Complex and the supracrustal Kinzigite Formation. The Mafic Complex comprises gabbroic, noritic and dioritic rocks which have intruded the metasedimentary sequences of the Kinzigite Formation (Sinigoi et al., 1991; Quick et al., 2003). The Kinzigite Formation is mainly composed of metapelites, interlayered with metagreywackes, metabasites, and minor marbles and quartzites (Schmid, 1993; Barboza & Bergantz, 2000; Quick et al., 2003).

Metapelites of the Kinzigite Formation show an increase in metamorphic grade from amphibolite facies in the SE to granulite facies in the NW (Schmid & Wood, 1976; Schmid, 1993; Henk, Franz, Teufel, & Oncken, 1997). Some studies have used the term "kinzigite" for amphibolite facies rocks and "stronalite" for rocks showing a granulite facies assemblage (Schnetger, 1994). The Kinzigite Formation of Val Strona di Omegna was subdivided into three zones: amphibolite facies, transition zone and granulite facies (Fig. 1b-d). Rocks from granulite facies zone are considered to have experienced extensive partial melting and melt loss (e.g., Schnetger, 1994, Sinigoi, Quick, Demarchi, & Klötzli, 1994; Redler, White, & Johnson, 2013). *P–T* conditions of metamorphism in Val Strona di Omegna have been widely investigated by conventional thermobarometry (Henk, Franz, Teufel, & Oncken, 1997; Bea & Montero, 1999), phase equilibria modeling (Redler, Johnson, White, & Kunz, 2012; Kunz, Johnson, White, & Redler, 2014; Redler et al., 2013) and trace element thermometry (Luvizotto & Zack, 2009; Ewing, Hermann, & Rubatto, 2013). Maximum *P–T* estimates calculated by Henk et al. (1997) and Bea & Montero (1999) are ≈800 °C and ≈8 kbar in the granulite facies zone (Fig. 1b). Based on phase equilibrium modeling, Redler et al. (2012) suggested that rocks from Val Strona di Omegna preserve a regional field gradient from 3.5-6.5 kbar at 650-730°C in the upper amphibolite zone, to 11-12 kbar, 900°C at granulites facies zone (Fig. 1b). Peak temperatures of 900-950°C are also inferred from Zr-in-rutile thermometry (Luvizotto & Zack, 2009; Ewing et al., 2013).

The relationship between the intrusion of the Mafic Complex and the granulite facies metamorphism has been largely debated. Some authors considered that the intrusion of mafic magmas may be the cause for the high-grade metamorphism (Sinigoi et al., 1991; Henk et al., 1997). However, other works have shown that mineral assemblages close to the intrusion preserve evidence of low-pressure (contact) metamorphism, and thus argue that the intrusion of mafic rocks occurred rather later (e.g. Barboza, Bergantz, & Brown, 1999; Barboza & Bergantz, 2000; Redler et al., 2012; Ewing et al., 2013). The regional metamorphism of amphibolite to granulites facies in the Ivrea Zone was firstly dated at 299 Ma (Vavra, Schmid, & Gebauer, 1999); later the age of 316 Ma was reported by Ewing et al. (2013). On the contrary, the intrusion of the Mafic Complex occurred during decompression at 288 Ma (Peressini et al., 2007) and caused an additional event of contact metamorphism around the intrusion (Barboza & Bergantz, 2000; Redler et al., 2012). A more recent work (Kunz, Regis, & Engi, 2018a) has demonstrated a long duration for the high temperature conditions in the Kinzigite Formation (300-240 Ma) and concludes that such long thermal history requires additional heat sources. The preferred geodynamic model suggests the upwelling of the asthenospheric mantle as the most conceivable source (e.g. Schaltegger et al., 2002; Kunz et al., 2018b).

3. METHODS

Samples were collected along the Val Strona di Omegna (Fig. 1a) and petrographic analyses conducted in order to select representative rocks from the three main zones (Fig. 1b-d). A detailed study was conducted in inclusions on 12 thin and doubly-polished thick (80-200 μm) sections using a light polarized microscope.

Back-scattered electron (BSE) imaging of the inclusions, together with and semi-quantitative energy dispersive spectroscopy (EDS), were carried out using a CAM SCAN MX3000, equipped with LaB6 cathode at the Dipartimento di Geoscienze, Università di Padova (Italy), and a Sigma Zeiss field emission scanning electron microscope (FESEM) equipped with Oxford XMax EDS Silicon Drifted detector at the CNR-IENI, Padova.

Major element concentrations of the minerals (garnet, muscovite and biotite) were determined on polished carbon-coated thin sections of 30 μm thickness using the CAMECA SX50 electron microprobe with five wavelength dispersive spectrometers at the C.N.R.-I.G.G. (Consiglio Nazionale delle Ricerche-Istituto di Geoscienze e Georisorse) Dipartimento di Geoscienze, Università di Padova, Italy. The operating conditions were: 20 nA beam current, 20kV acceleration voltage, and 5 μm beam diameter and counting times of 10s on peak and 5s on background. The composition of re-homogenized melt inclusions was determined using a JEOL JXA 8200 Superprobe at the Dipartimento di Scienze della Terra, Università di Milano, using 15 kV accelerating voltage, 5 nA beam current, 10 s on the peak and 5 s background, and 1 μm beam diameter to avoid contamination from the surrounding host. Alkali loss was estimated using leucogranitic standards showing a similar composition to the melts, and correction factors were applied for Na, K, Al and Si. Selected microprobe analyses of minerals from representative samples are given in Table 1, and composition of re-homogenized MI are given in Table 2.

Micro-Raman measurements were performed on five representative doubly-polished thick sections (STR69, IVT21, STR22, STR28 and STR36) at the Institute of Earth and Environmental Sciences (University of Potsdam), using a HORIBA Jobin-Yvon LabRAM HR 800 equipped with a Peltier cooled multichannel CCD detector and coupled with a petrographic microscope Olympus BX41. Raman spectra were recorded between 100 and 4000 cm^{-1}, using a 100x objective. Integration time of analyses was of 30 s and 3 accumulations, with a spectral resolution of 10 cm^{-1}.

Re-homogenization of the nanogranitoid inclusions was performed on garnet chips or cores separated from polished sections of various thicknesses (from 300 μm to 2 mm). Experiments were done using a single-stage piston cylinder at the Laboratory of Experimental Petrology, Dipartimento di Scienze della Terra, Università di Milano, Italy, using the method described by Bartoli et al. (2013b). Experimental re-melting of the inclusions was performed under the following conditions: 820°C – 1 GPa, 20h (sample STR36), 840°C – 1.2 GPa, 5h (sample STR28, experiments BC6 and BC9), 850°C – 1 GPa, 20h (sample IVT21, experiments IVT21 and IV21) and 900°C – 1.2 GPa, 5h (sample STR22, experiments BC8 and BC10). Shorter run durations (5 hours) were done in order to avoid interaction of the melt with the host garnet at higher temperatures. Pressures, generally higher with respect to those recently reported for Val Strona di Omegna (Fig. 1b; Redler et al., 2012), were chosen in attempt to exceed the internal pressure of inclusions during experimental remelting and avoid their decrepitation and volatile loss upon heating (cf. Figure 9 in Bartoli et al., 2013b).

Due to the very small size of the inclusions, the contents of H_2O and CO_2 of re-homogenized glasses were obtained using a CAMECA Nano Secondary Ion Mass Spectrometry 50 (NanoSIMS) at the Muséum National d'Histoire Naturelle of Paris following the procedure of Bartoli et al. (2014) and Créon, Levresse, Remusat, Bureau, & Carrasco-Núñez (2018). Experimental capsules with exposed re-homogenized inclusions were mounted in Indium to improve vacuum in the analysis chamber (Aubaud et al., 2007) and coated with Au. In order to remove the coating and reach sputtering steady-state, sample surface was presputtered by a Cs^+ primary beam set at 340 pA and rastered over 5×5 μm^2 surface area before each analysis. Analyses were performed using a 30 pA Cs^+ primary beam rastered over 3×3 μm^2 surface area. However, to avoid surface contamination only ions from the inner 1×1 μm^2 were collected using the "beam blanking" mode. Secondary ions of $^{12}C^-$, $^{16}OH^-$, $^{28}Si^-$ and $^{56}Fe^{16}O^-$ were collected in multicollection mode and used to identify the MI. Mass resolving power was set at minimum 6000, sufficient to resolve interferences on $^{16}OH^-$. A single analysis comprises a stack of 200 cycles, each cycle being 1.024 s long. The vacuum in the analysis chamber remained below 2×10^{-9} Torr during the session of H_2O and CO_2 measurements.

The H_2O and CO_2 contents of the glasses (Table 3) were determined through the measurement of $^{16}OH^-/^{28}Si^-$ and $^{12}C^-/^{28}Si^-$ ratios, respectively. These ratios were converted into concentrations using calibration curves determined using standards of known compositions. The standards used for the determination of H_2O contents were three leucogranitic glasses: DL reported in Acosta-Vigil, London, Morgan, & Dewers (2003) with H_2O = 6.5 wt.%; glass LGB1 from Behrens and Jantos (2001) with H_2O = 4.9 wt.%; and the almost anhydrous glass B from Morgan and London (2005) with H_2O = 300 ± 42 ppm. The standards used for the determination of CO_2 contents were four trachyandesitic standards (STR 9, 10, 11 and 13) from the Stromboli volcano experimentally doped in carbon and water by Bureau et al. (2003). Concentrations and uncertainties were determined using the R program following the procedure described in Bartoli et al. (2014) and Thomen, Robert, & Remusat (2014).

For phase equilibria modeling the model chemical system MnNCKFMASHT (MnO–Na_2O–CaO–K_2O–FeO–MgO–Al_2O_3–SiO_2–H_2O–TiO_2) was used with the normalized bulk rock composition in mol.% based on major element XRF analysis. The H_2O content was assumed on the basis of the measured LOI value. Fe_2O_3 was not considered owing to the very low amounts found by means of iron titration of Val Strona di Omegna samples (0.1 mol.%; Redler et al., 2011). To reconstruct a probable prograde history, the melt-reintegration approach has been applied on sample STR28 (Bartoli, 2017 and references therein). The amount of melt to be reintegrated has been chosen to bring the solidus to H_2O-saturated conditions at the pressure of 10 kbar. The melt composition, instead, has been obtained from re-melting experiments of nanogranitoids from sample STR28 (details on the procedure are reported in Bartoli, 2018). Calculations were done by the Gibbs energy minimization using the Perple_X 6.7.9 software (Connolly, 2009) with the thermodynamic database of Holland and Powell (2011). The solution models used are: melt from White, Powell, & Holland (2007), garnet from Holland and Powell (1998), biotite from Tajčmanová, Connolly, & Cesare (2009), white mica from Coggon and Holland (2002), plagioclase from Newton, Charlu, & Kleppa (1980) and K-feldspar from Thompson and Hovis (1979). An ideal model was used for cordierite and ilmenite.

4. RESULTS

4.1 Samples and petrography

Samples investigated in this study are metapelitic migmatites collected from the three main metamorphic zones of the Ivrea Zone, in Val Strona di Omegna (Fig. 1a): upper amphibolite facies (UA), transition zone (T) and granulite facies (G, see Fig. 1b-d). For further details on the field aspects of the three zones, the reader is referred to Redler et al. (2012), Redler, White, & Johnson (2013) and references therein.

In the UA zone, the studied rocks (STR36 and STR77) are metatexites with thin (up to ~5 mm) leucosomes (Fig. 2a) as patches or along the folded foliation. The melanosome is lepidoblastic, fine-grained, and comprises biotite (X_{Mg} 0.42; Ti 0.42 a.p.f.u.), fibrolitic sillimanite, quartz, plagioclase, small porphyroblasts of garnet, K-feldspar and minor relict of muscovite (X_{Mg} 0.46; Fig.

3a). Sample STR36 is located in the transition zone from Redler et al. (2012) (Fig. 1b,c), however it is compositionally and microstructurally similar to STR77, sampled at upper amphibolite zone. This is actually in agreement with the amphibolite zone proposed by Schmid (1993), in which case the transition zone is more restricted (Fig. 1d). An important accessory mineral is graphite which occurs in matrix together with ilmenite, apatite, tourmaline, zircon and monazite. Locally, biotite shows resorbed outlines and is associated to films of K-feldspar and quartz. Corroded muscovite may also occur. The garnet occurs as small (up to 1mm), subhedral crystals with abundant FI and NI (Fig. 3b,c), along with quartz, graphite, biotite and sillimanite. No significant zoning is observed in terms of major elements in the garnet, from rim ($Alm_{77}Sp_9Gr_6Prp_9$, X_{Mg}~ 0.11) to core ($Alm_{75}Sp_6Gr_4Prp_{13}$, X_{Mg}~ 0.15).

In the T zone, studied samples (STR28 and IVT21) are stromatic metatexites with variable amount of discontinuous, cm-sized, leucosomes which may contain large garnet crystals (Fig. 2b). The melanosome is strongly foliated (Fig. 3d), medium- to coarse-grained, composed of abundant biotite (X_{Mg} 0.5; Ti 0.54 a.p.f.u.), garnet, fibrolitic to prismatic sillimanite, K-feldspar, plagioclase and quartz. Muscovite is not present. Evidence for partial melting are resorbed biotite and sillimanite associated with films of K-feldspar and quartz (Fig. 3e). Accessory phases are graphite, ilmenite, apatite, zircon and monazite. The garnet crystals are much larger (<1 cm) than in UA zone, and contain clusters of FI and NI (Fig. 3d and f) in their core, together with quartz and graphite. From core ($Alm_{70}Sp_3Gr_4Prp_{22}$; X_{Mg}~ 0.24) to rim ($Alm_{78}Sp_4Gr_3Prp_{14}$; X_{Mg}~ 0.2), the garnet is slightly more almandine-rich.

In the G zone, the studied metapelites are residual diatexites (STR22 and STR69), in which the melanosome is mainly composed of coarse-grained garnet (0.5-1.2 cm) and prismatic sillimanite (Fig. 2c and 3g), and also plagioclase, K-feldspar, quartz and subordinated biotite (X_{Mg} 0.53; Ti 0.6 a.p.f.u.). Accessories in this case are graphite (relatively less abundant than in the samples from upper amphibolite and transition zones), apatite, zircon, monazite and rutile. Garnet occurs as elongate porphyroblasts with variable amounts of inclusions. FI and NI inclusions occur mostly in the cores (Fig. 3g) together with biotite, sillimanite, quartz, rutile and graphite, however these other phases may also be at rims. No significant zoning was observed from core ($Alm_{68}Sp_1Gr_5Prp_{26}$; X_{Mg}~0.28) to rim ($Alm_{72}Sp_2Gr_3Prp_{21}$; X_{Mg}~0.23).

4.2 Microstructural characterization of the inclusions

Garnet crystals from the three zones contain abundant inclusions and, as mentioned above, the characterization of the phases inside them was done by BSE imaging, EDS analysis and micro-Raman spectroscopy.

Petrography indicates the presence of two types of primary multiphase inclusions in the same clusters (Fig. 3b, c and f), regularly distributed in the cores of the garnet: one darker, with very high birefringence at cross-polarized light and another light-colored to transparent (Fig. 3f), with relatively lower birefringence (Fig. 3c). These are respectively FI and NI. Both types of inclusions have similar size (mostly 2-10 μm) and usually negative crystal shapes (Fig. 3f and 4a-e). Very few of them may show evidence of decrepitation such as small tails and microcracks (Fig. 4f).

Nanogranitoids contain aggregates of K-feldspar, plagioclase, quartz, biotite, muscovite, chlorite (Fig. 4a-d), and in some cases calcite (Fig. 4e). Micro-Raman investigation has indicated the presence of polymorphs such as kumdykolite ($NaAlSi_3O8$), cristobalite, trydimite (Fig. 5a-c), and, in one inclusion, kokchetavite ($KAlSi_3O_8$). Furthermore, a few inclusions may contain CH_4 and N_2 (Fig. 5d). Concerning the minerals crystallized from the melt, no variation in mineral assemblage was observed in the samples from the three zones. Common trapped minerals are graphite, apatite, zircon, and ilmenite, whereas rutile is observed frequently in inclusions from G, and rarely from T zone. Glassy inclusions or residual glass in NI were not detected.

The FI, darker under transmitted light (Fig. 6a), have very high birefringence under cross polarizers (Fig. 6b), and are composed of fluid and solid phases; the latter comprise both daughter and trapped minerals. These FI are more abundant in the UA metatexites suggesting that the fluid/melt ratio is higher in these rocks, when compared to the T zone and G rocks. Micro-Raman has shown variable proportions of CO_2, CH_4 and N_2 (Fig. 5e,f); no H_2O was detected. Amongst the most common phases identified in the inclusions are siderite, pyrophyllite (Fig. 6c) and kaolinite (Fig. 5f), and in a few cases calcite, magnesite and graphite. Rutile was observed in the samples from G and likely represents a trapped phase, since some terminations of rutile grains are partially enclosed in the host garnet. The FI throughout the three zones have variable compositions and densities, and different proportions of fluid phases are sometimes observed in the same sample. The relative amounts of components in the fluid were calculated using the method by Dubessy, Poty, & Ramboz (1989). For instance, at UA CO_2 (absent to 94 mol.%), N_2 (22 to 56 mol.%) and CH_4 (absent to 12 mol.%), at T, CO_2 (absent to 92 mol.%), N_2 (5 to 95 mol.%) and CH_4 (absent to 70 mol.%), and at G, CO_2 (absent to 86 mol.%), N_2 (18 to 23 mol.%) and CH_4 (absent to 76 mol.%). The CO_2 density of the inclusions was calculated using the method based on the measurement of the Raman intensity of the Fermi diad (Wang et al., 2011) and vary from 0.1 to 0.6 g/cm^3. These variable compositions and densities are interpreted as result of the interaction of fluid with the host during the cooling path of the migmatites (e.g. Kleinefeld & Bakker, 2002; Tacchetto et al., 2018; see below).

4.3 Microstructures of inclusions after re-melting experiments

The conditions for the re-melting experiments of samples from the three zones were chosen following the phase equilibria modelling from the literature (Redler et al., 2012). As expected all successful experiments showed the presence of homogeneous glass (i.e. melt; Fig. 7a-d). Together with the glass, some inclusions have shown the presence of graphite (Fig. 7e), which represents the most commonly observed phase in the studied samples, and in one sample, euhedral plagioclase (Fig. 7f) was also present. These phases were observed in inclusions before the experiments and are interpreted as trapped phases inside the melt inclusions, i.e. they were present together with the melt during entrapment (e.g. Acosta-Vigil et al., 2016). Bubbles may also be observed together with glass (Fig. 7g,h), and may result from incomplete dissolution of the fluid into the melt during the experiment, or may be shrinkage bubbles (Lowenstern, 1995).

Incomplete re-melting of some inclusions was also observed, and in that case corroded biotite occurs together with rounded crystals of quartz and glass (Fig. 7i). Interaction with the host was also observed in some cases, as suggested by irregular boundaries of remelted inclusions, formation of new phases such as orthopyroxene (Fig. 7j) and the host garnet showing a different composition in proximity of remelted inclusion (see contrasting shade of grey in the BSE, Fig. 7j).

4.4 Composition of anatectic melts

Major elements and CIPW normative diagrams

Approximately 130 EMP analyses were performed on the remelted MI. Analyses that have clearly shown evidence of interaction/contamination with the host were disregarded. Composition of the preserved inclusions were recalculated to an anhydrous basis and are described below (see Fig. 8 and Table 2).

The data show that all the melts in the three zones are granitic *s.l.*, peraluminous (Fig. 8a) and have similar ranges of silica (70-78 wt. %), Na_2O (2-4 wt. %) and Al_2O_3 (12.5-16.5 wt. %) in most cases. However, slightly differences in compositions can be noticed. In samples from the UA, melts have restricted K_2O (3.6-5.1 wt. %; Fig 8b), lower Na_2O/K_2O (0.4-0.9), and CaO (0.4-1.2 wt. %, Fig. 8c), are peraluminous (ASI ~ 1.1-1.5) and less mafic (FeO+MgO 2-3.4 wt. %; Fig 8d). The melts from T have more spread compositions, are more peraluminous (ASI ~ 1.1-1.8), have higher Na_2O/K_2O (0.1-1.2), and maficity (FeO+MgO 1.2- 3.9 wt. %). The melts at G are peraluminous (ASI ~ 1.2-1.3), have the lowest K_2O (1.8 to 2.5 wt. %) and reach highest Na_2O/K_2O (1.2-1.9), CaO (1.4-2.5 wt. %) and FeO+MgO (3.2-4.7 wt. %).

In the CIPW-normative Ab-An-Or diagram (Fig. 9a), the MI form two distinct groups, one including MI from UA and T, which are classified as granite, but show variable Ab/Or ratios and a second, more restricted group, represented by the MI from G which have lower Or contents and higher An contents, and are classified as granodiorites. When compared to other NI from the literature, the MI from UA and T have relatively higher An contents. In turn, the MI from G plot in the same field as MI from Kali Gandaki (Nepal) and Jubrique (Spain).

In the haplogranite system (Qz-Ab-Or, Fig. 9b), the MI also form two distinct groups. The MI from G have lower Or, and comparable compositions with MI from Kali Gandaki and Jubrique. The MI from UA and T display variable compositions, and are mostly similar to Ojen metatexites and diatexites (Spain). The spread of composition of MI from the three zones is mostly parallel to the Qz-

Ab sideline, and could be the effect of sluggish diffusion of SI and Al versus rapid diffusion of alkalis in the granitic melt (e.g. Acosta Vigil, London, & Morgan, 2006).

H_2O and CO_2 contents of the melts

The H and C concentrations, then recalculated as H_2O and CO_2, were measured on remelted inclusions from three zones (STR36 from UA, STR28 and IVT21 from T, STR22 from G); results are given in Table 3.

MI from all three zones span a wide range of concentrations of CO_2 (Fig. 9). The sample from UA varies from 861 to 1738 ppm (average 1384 ± 373 ppm), in which the lowest values were observed in an inclusion of glass coexisting with a bubble and the highest values were measured in homogeneous glass. Samples have the lowest contents of CO_2 in T, vary from 495 to 1165 ppm (IVT21) and 573 to 1534 (STR28), and have much lower averages (IVT21, 884 ± 267 ppm; STR28, 835 ± 329 ppm). In this case, both the lowest and highest values are not easily correlated to the presence of bubbles or crystals. Sample STR22 from G has two contrasting signatures, one similar to the previously described for T (BC8 from 739 to 901 ppm, average 833 ± 61 ppm), and another that displays the highest CO_2 values (BC10 from 1354 to 2444, average 1788 ± 395 ppm). The highest values occur when the glass coexists with graphite, whereas the lowest values occur in inclusions with homogeneous glass.

The highest H_2O contents were measured on the sample from UA (10 wt.%), and the lowest in the sample from T (STR28 4.8 wt.%). Average H_2O contents are progressively lower with increasing metamorphic grade: at UA values are slightly higher (8.1 ± 1.4 wt.%), at T, intermediate (7 ± 0.9 wt.%) and at G, lower (6.8 ± 0.7 wt.%). However, the ranges of the three zones are relatively similar (UA 6.5 to 10 wt.%; T 4.8 to 8.5 wt. %; G 5.4 to 8.2 wt.%; see Fig. 9).

6. Discussion

6.1 Significance of melt and fluid inclusions

Our study of inclusions of the metapelitic migmatites from the Val Strona di Omegna (IZ) has shown the coexistence of NI and FI inclusions in clusters regularly distributed in the cores of the garnet (Fig. 3). Such microstructural evidence suggests a primary coeval entrapment during the growth of peritectic garnet (Roedder, 1979; Cesare et al., 2015), i.e. these two different types of inclusions are related to the same anatectic event.

Considering the mineral assemblages, their behavior during experimental remelting and their chemical composition, NI can be reliably interpreted as former droplets of felsic silicate melt. The presence of polymorphs such as kumdykolite, cristobalite, trydimite and kokchetavite has been previously reported as evidence for the preservation of the original composition of the inclusions (e.g. Ferrero et al., 2016a; see also Ferrero & Angel, 2018) including the volatiles such as H_2O and CO_2. Indeed, these polymorphs are highly susceptible to transformation into their thermodynamically stable phases as result of inclusion decrepitation. Therefore, their occurrence in the investigated NI from Val Strona di Omegna suggests that the inclusions represent a reliable source of information on the starting composition of the anatectic melts and fluid regime of the IZ.

Fluid inclusions described in this study are composed of variable proportions of CO_2, N_2 and CH_4, along with siderite, pyrophyllite and kaolinite as daughter phases. This strongly indicates that, although the initial composition was not determined here, the fluid present during anatexis had a COHN composition. The variable compositions and densities of the FI are interpreted as result of post-entrainment re-speciation and reaction between host garnet and the fluid during the cooling path of the migmatites (e.g. Kleinefeld & Bakker, 2002; Ferrero et al., 2014; Tacchetto et al., 2018), which resulted in the crystallization of daughter phases. A possible reaction in the Fe end-member system would be:

$$\text{Almandine} + 1.5\ H_2O + 3\ CO_2 = 3\ \text{Siderite} + 0.5\ \text{Pyrophilite} + 0.5\ \text{Kaolinite}$$

Primary in origin, the investigated NI and FI represent, therefore, snapshots of coexisting anatectic melt and C-bearing fluid which were present during partial melting of this section of deep continental crust; i.e., they are indicative of a situation of immiscibility between a carbonic fluid and a crustal melt which may result from the low solubility of carbonic fluid in granitic melts (e.g. Cesare and Maineri, 1999; Tamic, Behrens, & Holtz, 2001).

The possibility for peritectic garnet to trap droplets of coexisting melt is highlighted by phase equilibria modelling of a probable protolith composition in which garnet and melt modes rapidly increase after crossing the solidus (Fig. 11a). In a situation of fluid-melt immiscibility, the growing garnet would be obviously able to trap both melt and fluid.

The phase diagram of Figure 11a was constructed without considering the presence of a COH fluid. Despite the recent advances in the calculation of partial melting equilibria (White et al., 2011; Palin et al., 2016; White, Palin, & Green, 2017), the suprasolidus behaviour of graphitic systems cannot be adequately modelled owing to the lack of a melt model that considers the occurrence of carbonic species (both CO_2 and CH_4) (see discussion in Bartoli et al., 2016). In this sense, NI and FI in peritectic minerals represent a unique natural laboratory to recover melting mechanisms in deep crustal rocks.

6.2 New clues on anatexis of the Ivrea Zone

The Ivrea Zone (NW Italy) is a world-renowned Permian mid to lower crustal section. Crustal rocks have been widely investigated through all possible approaches such as field observations (e.g., Zingg, 1980; Quick et al., 2003; Redler et al., 2012, 2013), phase relationships (e.g., Schmid & Wood, 1976), fluid inclusions (De Negri & Touret, 1978), whole rock geochemistry (major and trace elements and isotopes; e.g., Sighinolfi & Gorgoni, 1978; Baker, 1988; Schnetger, 1994; Henk et al., 1997; Barboza et al., 1999; Bea & Montero, 1999; Alessio et al., 2018), conventional thermobarometry (e.g., Schmid & Wood, 1976; Zingg, 1980; Sills, 1984; Henk et al., 1997; Demarchi et al., 1998; Bea & Montero, 1999; Barboza & Bergants, 2000), geochronology (Köppel, 1974; Vavra et al., 1999; Ewing et al., 2013, 2015; Klötzli et al., 2014; Kunz et al., 2018a, b), trace element thermometry (Luvizotto & Zack, 2009; Ewing et al., 2013; Kunz et al., 2018) and modern phase equilibria modelling (Redler et al., 2012, 2013; Bartoli, 2018). Despite the impressive number of studies devoted to reconstruct the high-temperature and anatectic history of this deep crustal section, the first and clear evidence of carbonic fluid-present melting in the Ivrea Zone is reported only in this study.

There is some discrepancy among published *P–T* estimates for the rocks in Val Strona di Omegna (Fig. 1b). Successful remelting experiments of nanogranioids may provide an additional and realistic constraint on the conditions, in particular the temperature, at which melt was present in the system; i.e., at which rocks were partially melted (Bartoli et al., 2013b; Bartoli, Tajcmanová, Cesare, & Acosta-Vigil, 2013c; Ferrero et al., 2015). Experimental remelting performed in this study indicates that garnet grew and trapped melt inclusions between 820 and 900 °C, proving that UHT conditions were approached in this section on continental crust and confirming the estimates based on trace element thermometry and phase equilibria calculations (Redler et al., 2012; Luvizzotto & Zack, 2009; Ewing et al., 2013). Conversely, conventional exchange and net transfer thermobarometry gave ≈130-170 °C lower and ≈2-4 kbar lower values (Fig. 1b; see above). This discrepancy is likely to be related to a significant retrograde re-equilibration of mineral compositions (Pattison et al., 2003; Redler et al., 2012).

According to the literature, the rocks from IZ have experienced anatexis through fluid-absent breakdown of muscovite and biotite, and extensive partial melting at the highest temperatures (up to 40–50 vol.% melt at 850-900 °C) (Fig. 11b; see also Schmid & Wood, 1976; Schnetger, 1994; Sinigoi et al., 1994). In this study, we have shown that the microstructural evidences for anatexis include the presence of corroded muscovite (restricted to some samples from amphibolite facies), but more frequently biotite with resorbed outlines associated with films of K-feldspar and quartz, and NI in peritectic garnet (e.g. Cesare et al., 2015), which are found from UA to G (e.g. all samples in Fig. 1b). Thus, incongruent melting of biotite in the metapelitic migmatites and the formation of peritectic garnet may have started before the muscovite-out isograde (sample 77, Fig. 1b). Our phase equilibrium modelling (Fig. 11a) shows that continuous melting of biotite <800°C produces garnet and melt. Another possibility could be that the breakdown of muscovite may also have produced small proportions of garnet with the melt, similar to the migmatites from Ronda (Bartoli, Tajcmanová, Cesare, & Acosta-Vigil, 2013c). Moreover, the primary microstructural arrangement of NI and FI suggests that anatexis of these metapelites occurred through breakdown melting of muscovite and biotite but always in the presence of a COH fluid, as expected from theoretical considerations on the behavior of graphitic systems (see discussion for the origin of the fluid below).

The composition of the melts from UA and T are similar and consistent with melting of biotite, in agreement with microstructural observations and phase equilibria constraints (Figs. 3 and 11). On the other hand, the melts from G display higher contents of CaO, lower K_2O (and consequently higher normative An and lower Or contents) and higher FeO+MgO (Figs. 8, 9).

Most of the MI analysed in this study have FeO+MgO contents <3 wt.% similar to other MI from the literature (see Cesare et al., 2015). However, 40% of MI from the T and all from G have FeO+MgO from 3 to 4.7 wt.%. Same ranges are observed in MI from terranes where anatexis occurred at 850-900°C (e.g. El Hoyazo, Bohemian Massif and Kerala Khondalite belt). This is consistent with experimental works which suggest that temperature controls the FeO+MgO and CaO of the melts (Johannes & Holtz, 1996; Montel & Vielzeuf, 1997; Gao et al., 2016).

Higher CaO and FeO+MgO in MI might indicate that melts have interacted with the host, and therefore they could not represent pristine compositions. These cases can be detected if the host garnet has higher contents of Ca and positive correlation of FeO+MgO and ASI in the MI is observed (e.g. Cesare et al., 2015). However, contents of Ca in the garnet are virtually the same in the three zones (see Table 1), furthermore, correlation between FeO+MgO and ASI does not occur. Therefore, compositions of remelted MI from G are interpreted to be original, and not related to interaction between melt and host. The contrasts in the compositions of the MI from UA facies and T versus G can be related to several additional factors, we discuss some of them below.

All remelted inclusions from this study have higher normative An contents then most MI from the literature (see Fig. 9a). The highest An contents are observed in the melts from G, which are compositionally granodiorites, and plot together with MI from Kali Gandaki (Nepal) and Jubrique (Spain). More calcic compositions of crustal melts have previously been interpreted as a result of H_2O present-melting (Patiño Douce & Harris, 1998; Frost & Frost, 2008), and likewise these two occurrences mentioned above were interpreted to have been formed by fluid present melting (T<800°C) (Carosi et al., 2015; Acosta-Vigil et al., 2016). This is coherent in the case of MI from Jubrique, which have high H_2O contents (7 to 13 wt.%) and low FeO+MgO (Acosta-Vigil et al., 2016). However, the MI from G are unlikely to have been produced under similar conditions. Indeed, the H_2O contents of melts are lower despite the higher P of formation, and there is no evidence, in terms of FI, of the presence of free water at suprasolidus conditions.

Garcia-Arias (2018) recently showed a mismatch between the Ca contents and maficity of anatectic melts and S-type granites, and concluded that preferential non-stoichiometric entrainment of plagioclase could be a viable process to increase the Ca of granitic magmas. However, our data, coming from MI that cannot have been influenced by entrainment, show that under some circumstances, anatexis may produce primary melts with higher Ca and maficity.

Alternatively, Ca-rich compositions could result from changes in the reactants, for example, a greater contribution of (Ca-rich) plagioclase at granulite facies. A similar scenario, in which rims of plagioclase may melt congruently producing a more Ca-rich melt, was considered by Taylor et al. (2014) in order to explain composition of the K-poor, Ca-rich leucosomes of the Southern Marginal Zone migmatites, Limpopo Belt, South Africa. Thus, we believe that the MI from granulite facies may represent an additional evidence for the origin of Pl-rich leucosomes usually found in granulite terranes (e.g. Sawyer et al., 1999; Taylor & Stevens, 2010). However, detailed study of the microstructure of leucosomes is necessary in order to evaluate if the low K and high Ca was not produced by cooling driven processes, for instance, framework of plagioclase may indicate loss of interstitial (fractionated) melt (e.g. Carvalho et al., 2016).

The breakdown of apatite (and monazite) during suprasolidus metamorphism of metapelites is the main supplier of phosphorus, as well as LREE, to the anatectic melt (see Yakymchuk, 2017 for a review). Due to the high contents of Ca in apatite (~55 wt. % CaO), its dissolution could also have a influence on the contents of Ca of the melts. A detailed study of the accessory phases (monazite, zircon, apatite and xenotime) in the metapelitic migmatites from Val Strona di Omegna (Bea & Montero, 1999) showed that the grain size and modal abundance of apatite "decreases dramatically" in the rocks from granulite facies (so called stronalites by those authors; see their Table 1 and Figure 4), whereas in rocks from amphibolite and transition zones the grains are large and fairly abundant. Those authors interpreted this as result of elevated solubility of apatite in peraluminous melts. Thus, apatite may have played a (restricted) role and contributed to the Ca-budget (together with P_2O_5 and LREE) of the melts at G. Additional information on the trace elements and P_2O_5 of the melts (which were not analysed in this study) are required to further investigate this hypothesis.

Ca-rich and K-poor crustal melts were documented as leucosomes in the Kinzigite Formation of IZ. However, these rocks are restricted to the 2–3 km wide aureole around the Mafic Complex and are in textural equilibrium with cordierite and hercynitic spinel (Barboza et al., 1999; Barboza & Bergants, 2000). Instead, the investigated NI clearly coexist with peritectic garnet and come from metapelitic migmatites of Val Strona di Omegna which lack any clear evidence for a metamorphic overprint caused by the Mafic Complex (Redler et al., 2012). Therefore, the K-poor melt inclusions described in our study could likely represent crustal melts produced during HT-UHT regional metamorphism.

6.3 Immiscible carbonic fluids and the origin of CO_2-bearing fluid

We have shown that throughout the investigated anatectic rocks of the Ivrea Zone, peritectic garnet contains FI coexisting with NI, where the fluid is dominated by CO_2, CH_4 and N_2, without detectable H_2O. As suggested above, the original composition and density of such immiscible fluid within FI has been modified by both interaction with the host (e.g., Tacchetto et al., 2018) and re-speciation (e.g., Cesare, 1995) during cooling, leading to the formation of carbonates, graphite and phyllosilicates. Regardless of the actual fluid composition at the time of entrapment - which is beyond the scope of this research - a carbonic component must have been present (and abundant).

In addition, the contents of CO_2 (500 to 2500 ppm) found in the remelted inclusions from IZ are in agreement with the experiments of Tamic et al. (2001), and also represent a strong indication of the presence of a COH fluid during anatexis of the studied terrane. A similar scenario has been previously described by Cesare et al. (2007) in graphitic enclaves from El Hoyazo, where the fluid was considered internally derived. Another example of immiscibility was reported by Ferrero et al. (2014), however this case the fluid was interpreted to have derived from the crystallization of mantellic magmas (e.g. Touret, 1992).

The occurrence of CO_2-rich fluid inclusions in granulites is not an uncommon feature and the origins of the fluid, if externally or internally derived, have been described in several works (e.g. Huizenga & Touret, 2012, and references therein).

Frequently proposed sources of CO_2 in granulitic terranes are the degassing mantle and the crystallizing mantle-derived magmas which intruded the lower crust; i.e., externally derived CO_2 (Newton, 1980; Jackson, Mattey, & Harris, 1988; Touret, 1992; Santosh & Omori, 2008). In the IZ mafic magmas and deep crustal rocks coexist and the emplacement and crystallization of the Mafic Complex could have promoted the CO_2 flushing into the overlying Kinzigite Formation. However, the container of NI and FI (the peritectic garnet) is thought to represent part of the mineral assemblage related to the regional metamorphism whose thermal peak predates the emplacement of mafic magmas (Barboza et al., 1999; Barboza & Bergantz, 2000).

One could argue that the relationship between Mafic Complex and high-grade metamorphism of the Kinzigite Formation has long been debated and that some doubts still exist (Sinigoi et al., 1991; Henk et al., 1997; Vavra et al., 1999). Baker (1988) conducted an oxygen and carbon isotope study of minerals and rocks from Val Strona di Omegna and concluded that there is no evidence for significant transfer of CO_2-rich fluids from mantle to crust. Whatever the role of Mafic Complex is in the thermal history of the Kinzigite Formation, the infiltration of CO_2 from crystallizing mafic magmas is, therefore, highly improbable.

The metapelitic migmatites from IZ contain considerable amounts of graphite, therefore an internal origin for, at least, part of the carbonic component in the fluid is expected. Such COH fluid is initially produced by devolatilization of hydrous silicates (implied by the presence of graphite in the protolith, e.g. Connolly & Cesare, 1993), before or during amphibolite-facies metamorphism, explaining the higher fluid/melt in the rocks ratio from UA. With temperature increasing at suprasolidus conditions, a possible additional internal source might be the Fe^{3+} reduction during biotite melting accompanied by the oxidation of carbon and formation of CO_2 (Hollister, 1988; Cesare, Meli, Nodari, & Russo, 2005). The role of decarbonation in the marbles intercalated in the Kinzigite Formation cannot be completely excluded, however, it is probably unrelated (e.g. De Negri and Touret, 1978).

6.4 Implications for fluid regime of a high-grade terrane

Fluid regime during high-temperature metamorphism and crustal anatexis has been part of a heated ongoing debate in the literature. In the 1970s and early 1980s some seminal studies presented the concepts of "dehydration melting" and "fluid-absent melting" (Eggler, 1973; Thompson & Tracy, 1979; Thompson, 1982). These two terms imply that the melting process and formation of anatectic melt occur in absence of a fluid phase, through melting reactions involving the breakdown of hydrous minerals such as micas and amphibole. Fluid-absent conditions have been long considered to prevail during granulite-facies metamorphism, anatexis of the deep crust and formation of large volumes of crustal magmas (e.g., Clemens and Vielzeuf, 1987; Clemens & Watkins, 2001; Brown, 2013).

This point of view has been recently challenged by some works, which have highlighted the potential role of free H_2O and/or highly saline solutions (brines) during melting of the continental crust: water-fluxed melting (Weinberg & Hasalova, 2015a) and brine-assisted melting (Aranovich et al., 2014). Not surprisingly, these studies have added fuel to the fire. To have an idea of the heated debate in the scientific community, the reader may refer to Clemens and Stevens (2015) vs. Weinberg and Hasalova (2015b), and Aranovich Makhluf, Manning, Newton, & Touret (2016) vs. Clemens, Buick, & Stevens (2016). It is important to highlight the fact that despite there seem to be two opposite views on fluid regime during crustal melting, the fluid-present and -absent processes aren't mutually exclusive, and it is quite likely that during natural anatexis a transition from fluid-present to fluid-absent conditions often takes place (e.g., Acosta-Vigil et al., 2016). This view may hold in non-graphitic protoliths (see below).

An older, but still ongoing, controversy on the fluid regime in the deep continental crust is related to the existence of CO_2-rich fluids as well as their active role during high-grade metamorphism. The concept of "carbonic metamorphism" was firstly proposed by Newton et al. (1980). This theory derived from the observation of CO_2 fluid inclusions in many granulitic terranes (e.g., Touret, 1971) and invokes the flushing of CO_2-rich fluids to generate dry mineral assemblages typical of the granulitic crust. Despite the growing list of high-grade metamorphic terranes containing CO_2 fluid inclusions (Santosh & Omori, 2008; Huizenga & Touret, 2012; Touret & Huizenga, 2012;

and references therein), late relative ages of some inclusions (Lamb, Valley, & Brown, 1987), experimental constraints (Clemens, 1990) and the low mobility of CO_2 along grain boundaries (Watson & Brenan, 1987) raised serious doubts for this model. For example, Stevens & Clemens (1993) state that "…even when CO_2-rich fluid inclusions do record primary fluid compositions, this is not necessarily evidence for fluid-present conditions. Rather, in anatectic rocks, these inclusions represent the unreactive volatile dregs that would have occurred as high-dihedral angle bubbles in the granulite-grade environment". Clemens et al. (2016) reaffirm the same concept: "the presence of inclusions of such a fluid does not represent evidence for a truly fluid-present condition, as the rocks in which they occur would have behaved as fluid-absent bulk systems".

Because the IZ experienced high-grade metamorphism, up to granulite-facies conditions, and extraction of large volumes of crustal melt (reference here), it is considered an ideal natural laboratory to study melting processes which led to crustal differentiation and S-type granite formation (e.g., Sighinolfi & Gorgoni, 1978; Schnetger, 1994; Bea & Montero, 1999; Ewing et al., 2014; Alessio et al., 2018).

The CO_2-bearing inclusions investigated in this work are clearly primary in origin and related to the prograde history of these rocks (see above). The coexistence of NI and FI in peritectic garnet, their presence throughout the three zones and the measured CO_2 contents in NI unequivocally prove that the fluid regime during high-temperature metamorphism and anatexis in this Permian crustal section was characterized by the presence of a CO_2-bearing fluid phase. The fluid had progressively lower aH_2O from UA to G. Consistently, the contents of H_2O decrease in the melt, whereas CO_2 increases from UA to G (see above). The H_2O contents of the melts throughout the three zones in IZ indicate that aH_2O decreases with increasing metamorphic grade. AT UA, melts reach the highest values (6.5 to 10 wt.%), and decreases through T (4.8 to 8.5 wt.%) to G (5.4 to 8.2 wt.%). The melts are clearly H_2O-undersaturated, nevertheless, these values are slightly above the minimum water contents estimated for haplogranite systems at similar P-T conditions (respectively, 5, 4.5 and 4 wt.%; Holtz et al., 2001) which is usually assumed as initial H_2O contents of anatectic melts.

Although the study of nanogranitoids is still in its infancy (Cesare et al., 2015), the coexistence of NI and carbonic FI has been already documented in other regional, granulite-facies metamorphic terranes. Ferrero et al. (2016b) found silicate melt inclusions coexisting in the same cluster with carbonatitic inclusions and COH fluid inclusions in garnet from Bohemian Massif, indicating conditions of primary immiscibility between two melts and a fluid during the Variscan anatexis. Instead, Tacchetto et al. (2018) proved the presence of a CO_2-rich fluid during the Neoarchean anatexis of the continental lower crust exposed in the Athabasca granulite terrane (Canada). Additional examples of C-bearing fluid-melt immiscibility during prograde melting are documented in crustal enclaves from El Hoyazo (Spain) and La Galite (Tunisia) (Cesare et al., 2007; Ferrero et al., 2011, 2014).

Note that in many of these occurrences (Ivrea zone, Athabasca granulite terrane and El Hoyazo), plus several more unpublished (F. Ferri, unpublished data), graphite is present in the metasedimentary protolith. Owing to the differential partitioning fluid species (mainly H_2O, CO_2 and CH_4) between coexisting fluid and silicate melt, equilibrium thermodynamics impose that a rock undergoing melting will always show the presence of a free COH fluid, in variable amounts and with variable a_{H2O} depending on pressure, temperature and the bulk composition of the system (that can be expressed also as f_{O2}; Connolly & Cesare, 1993). It follows that not surprisingly, graphitic metasedimentary rocks behave in a fluid-present manner during anatexis, but that such fluid cannot be pure H_2O but rather a COH fluid. Consequently, in the same rocks the source of carbon is, at least in part, necessarily internal to the system, and that a possible mantle contribution, to be constrained by isotopic means, may also be an additional carbon source.

The role of COH fluids during high-temperature metamorphism and formation of granitic magmas has been largely discredited. Following Stevens & Clemens (1993), Clemens & Watkins (2001) state that "it is perfectly possible to have fluid-absent partial melting in the presence of graphite. For a treatment of this situation see Holloway et al., (1992)" and that "… graphite is unlikely to be ubiquitous in crustal protoliths of granitoid magmas. At granulite-facies temperatures, it is only likely to be stable in certain metapelitic rocks."

However, the study of Holloway and coworkers finds little, if any, applicability to the evolution of graphitic metapelitic systems which undergo breakdown of hydrous minerals. Holloway et al. (1992) presented an experimental study considering a hydrogen-free basaltic system in which the

CO_2 is produced by reaction between the graphite capsule and the Fe_2O_3 in the melt. Clearly a topic unrelated with the melting of metasediments in nature. Concerning the second issue highlighted by Clemens & Watkins (2001) - the scarcity of graphitic granulites, - we think that such a statement is in apparent contrast with evidence coming from graphitic granulite terranes worldwide, as attested by the vastness of literature on this topic indexed in the major publication databases.

We conclude that carbonic fluid-present melting of the deep continental crust may be more common than previously assumed and, together with breakdown melting reactions, it can represent an important key process in the origin of crustal anatectic granitoids. It follows that the nature of fluid regime during formation of granitic magmas may be variable and needs to be revaluated. In order for a reliable thermodynamic modelling to be possible, a more rigorous theoretical background and a comprehensive experimental dataset on the suprasolidus partitioning of H_2O, CO_2 and CH_4 between fluid and silicate melt are necessary and need to be implemented in the existing modelling softwares.

8. Conclusions

The study of nanogranitoid and fluid inclusions suggests that anatexis of the migmatitic metapelites from Ivrea Zone occurred through muscovite and biotite breakdown melting in the presence of a COH fluid. The fluid is assumed to be internally derived, produced initially by devolatilization of hydrous silicates in the graphitic protolith, then as result of oxidation of carbon by melting of Fe^{3+}-bearing biotite.

Composition of the melts vary with increasing metamorphic grade, and are interpreted to result from combination of higher T of melting, biotite melting in the three zones, but with greater contribution of anhydrous reactants (such as plagioclase) and minor role of apatite at granulite facies.

The aH_2O of the fluid dissolved in granitic melts decreases with increasing metamorphic grade. However, the H_2O contents of the melts throughout the three zones are comparable and slightly above than the minimum H_2O contents assumed. The CO_2 contents are highest at granulite facies, and show that carbon-contents of crustal magmas may not be completely negligible. Our data shows that the thorough investigation of melt inclusions may provide significant new information of well-studied terranes.

Acknowledgements

We thank Tanya Ewing for providing sample IVT21, and Alice Turina for providing samples and field data. We are in debt to Leonardo Toro for his support and assistance with the preparation of polished sections. Technical assistance from Raul Carampin (University of Padova) and Andrea Rispledente (University of Milano) during various analyses is really appreciated. The National NanoSIMS facility at the MNHN was established by funds from the CNRS, Région Ile de France, Ministère délégué à l'Enseignement supérieur et à la Recherche, and the MNHN. We are really grateful to Adriana Gonzalez-Cano for her support during NanoSIMS analyses.

FUNDING

This research was funded by a SIR RBSI14Y7PF grant to Omar Bartoli and XX grant to Fabio Ferri.

References

Acosta-Vigil, A., London, D., Morgan, G. B., & Dewers, T. A. (2003). Solubility of excess alumina in hydrous granitic melts in equilibrium with peraluminous minerals at 700–800 C and 200 MPa, and applications of the aluminum saturation index. *Contributions to Mineralogy and Petrology*, 146, 100-119.

Acosta-Vigil, A., London, D., & Morgan, G. B. (2006). Experiments on the kinetics of partial melting of a leucogranite at 200 MPa H_2O and 690–800 C: compositional variability of melts during the onset of H 2 O-saturated crustal anatexis. *Contributions to Mineralogy and Petrology*, 151, 539.

Acosta-Vigil, A., Barich, A., Bartoli, O., Garrido, C. J., Cesare, B., Remusat, L., Poli, S., & Raepsaet, C. (2016). The composition of nanogranitoids in migmatites overlying the Ronda peridotites

(Betic Cordillera, S Spain): the anatectic history of a polymetamorphic basement. *Contributions to Mineralogy and Petrology*, 171, 24.

Acosta-Vigil, A., London, D., VI, G. B. M., Cesare, B., Buick, I., Hermann, J., & Bartoli, O. (2017). Primary crustal melt compositions: Insights into the controls, mechanisms and timing of generation from kinetics experiments and melt inclusions. Lithos, 286, 454-479.

Alessio, K. L., Hand, M., Kelsey, D. E., Williams, M. A., Morrissey, L. J., & Barovich, K. (2018). Conservation of deep crustal heat production. *Geology*, 46, 335-338.

Aranovich, L. Y., Makhluf, A. R., Manning, C. E., & Newton, R. C. (2014). Dehydration melting and the relationship between granites and granulites. *Precambrian Research*, 253, 26-37.

Aranovich, L. Y., Makhluf, A. R., Manning, C. E., Newton, R. C., & Touret, J. L. R. (2016). Fluids, Melting, Granulites and Granites: A Controversy--Reply to the Commentary of JD Clemens, IS Buick and G. Stevens. Precambrian Research, 278, 400-404.

Aubaud, C., Withers, A. C., Hirschmann, M. M., Guan, Y., Leshin, L. A., Mackwell, S. J., & Bell, D. R. (2007). Intercalibration of FTIR and SIMS for hydrogen measurements in glasses and nominally anhydrous minerals. *American Mineralogist*, 92, 811-828.

Baker, A. J. (1988): Stable isotope evidence for limited fluid infiltration of deep crustal rocks from the Ivrea Zone, Italy. *Geology*, 16, 492-495

Barboza, S. A., Bergantz, G. W., & Brown, M. (1999). Regional granulite facies metamorphism in the Ivrea zone: Is the Mafic Complex the smoking gun or a red herring?. *Geology*, 27, 447-450.

Barboza, S.A., & Bergantz, G.W. (2000). Metamorphism and anatexis in the mafic complex contact aureole, Ivrea zone, northern Italy. *Journal of Petrology*, 41, 1307–1327.

Bartoli, O., Cesare, B., Poli, S., Bodnar, R.J., Acosta-Vigil, A., Frezzotti, M.L., & Meli, S. (2013a). Recovering the composition of melt and the fluid regime at the onset of crustal anatexis and S-type granite formation. *Geology*, 41, 115–118.

Bartoli, O., Cesare, B., Poli, S., Acosta-Vigil, A., Esposito, R., Turina, A., Bodnar, R.J., Angel, R.J., & Hunter, J. (2013b). Nanogranite inclusions in migmatitic garnet: behavior during piston-cylinder remelting experiments. *Geofluids*, 13, 405-420.

Bartoli, O., Tajčmanová, L., Cesare, B., & Acosta-Vigil, A. (2013c). Phase equilibria constraints on melting of stromatic migmatites from R onda (S. S pain): insights on the formation of peritectic garnet. *Journal of Metamorphic Geology*, 31, 775-789.

Bartoli, O., Acosta-Vigil, A., Ferrero, S., & Cesare, B. (2016). Granitoid magmas preserved as melt inclusions in high-grade metamorphic rocks. *American Mineralogist*, 101, 1543-1559.

Bartoli, O. (2017). Phase equilibria modelling of residual migmatites and granulites: An evaluation of the melt-reintegration approach. *Journal of Metamorphic Geology*, 35, 919-942.

Bartoli, O. (2018). Reintegrating nanogranitoid inclusion composition to reconstruct the prograde history of melt-depleted rocks. *Geoscience Frontiers*. doi: 10.1016/j.gsf.2018.02.002

Bea, F., & Montero, P. (1999). Behavior of accessory phases and redistribuition of Zr, REE, Y, Th, and U during metamorphism and partial melting of metapelites in the lower crust: an example from the Kinzigite Formation of Ivrea-Verbano Zone, NW Italy. *Geochimica et Cosmochimica Acta*, 63, 1133-1153.

Behrens, H., & Jantos, N. (2001). The effect of anhydrous composition on water solubility in granitic melts. *American Mineralogist*, 86, 14–20.

Brown, M. (2013). Granite: From genesis to emplacement. *Geological Society of America Bulletin*, 125, 1079-1113.

Brown, C. R., Yakymchuk, C., Brown, M., Fanning, C. M., Korhonen, F. J., Piccoli, P. M., & Siddoway, C. S. (2016). From source to sink: Petrogenesis of Cretaceous anatectic granites from the Fosdick migmatite–granite complex, West Antarctica. *Journal of Petrology*, 57, 1241-1278.

Bureau, H., Trocellier, P., Shaw, C., Khodja, H., Bolfan-Casanova, N., & Demouchy, S., (2003). Determination of the concentration of water dissolved in glasses and minerals using nuclear microprobe. Nucl. Instrum. Methods Phys. Res., Sect. B 210, 449–454.

Carosi, R., Montomoli, C., Langone, A., Turina, A., Cesare, B., Iaccarino, S., ... & Ronchi, A. (2014). Eocene partial melting recorded in peritectic garnets from kyanite-gneiss, Greater Himalayan Sequence, central Nepal. *Geological Society, London, Special Publications*, 412, SP412-1.

Carvalho, B. B., Sawyer, E. W., & Janasi, V. A. (2016). Crustal reworking in a shear zone: transformation of metagranite to migmatite. *Journal of Metamorphic Geology*, 34, 237-264.

Carvalho, B. B., Sawyer, E. W., & Janasi, V. A. (2017). Enhancing maficity of granitic magma during anatexis: entrainment of infertile mafic lithologies. *Journal of Petrology*, 58, 1333-1362.

Cesare, B. (1995). Graphite precipitation in C—O—H fluid inclusions: closed system compositional and density changes, and thermobarometric implications. *Contributions to Mineralogy and Petrology*, 122, 25-33.

Cesare, B., Meli, S., Nodari, L., & Russo, U. (2005). Fe^{3+} reduction during biotite melting in graphitic metapelites: another origin of CO_2 in granulites. *Contributions to Mineralogy and Petrology*, 149, 129-140.

Cesare, B., Maineri, C., Toaldo, A. B., Pedron, D., & Vigil, A. A. (2007). Immiscibility between carbonic fluids and granitic melts during crustal anatexis: a fluid and melt inclusion study in the enclaves of the Neogene Volcanic Province of SE Spain. *Chemical Geology*, 237, 433-449.

Cesare, B., Ferrero, S., Salvioli-Mariani, E., Pedron, D., & Cavallo, A. (2009). "Nanogranite" and glassy inclusions: The anatectic melt in migmatites and granulites. Geology, 37(7), 627-630.

Cesare, B., Acosta-Vigil, A., Bartoli, O., & Ferrero, S. (2015). What can we learn from melt inclusions in migmatites and granulites?. *Lithos*, 239, 186-216.

Chappell, B. W., White, A. J. R., & Wyborn, D. (1987). The importance of residual source material (restite) in granite petrogenesis. *Journal of Petrology*, 28, 1111-1138.

Clemens, J. D., & Vielzeuf, D. (1987). Constraints on melting and magma production in the crust. Earth and Planetary Science Letters, 86(2-4), 287-306.

Clemens, J. D. (1990). The granulite—granite connexion. In: Granulites and crustal evolution (pp. 25-36). Springer, Dordrecht.

Clemens, J., & Watkins, J. M. (2001). The fluid regime of high-temperature metamorphism during granitoid magma genesis. *Contributions to Mineralogy and Petrology*, 140, 600-606.

Clemens, J. D. & Stevens, G. (2012). What controls chemical variation in granitic magmas?. *Lithos*, 134, 317-329.

Clemens, J. D., & Stevens, G. (2015). Comment on'Water-fluxed melting of the continental crust: A review'by RF Weinberg and P. Hasalová. *Lithos*, 234, 100-101.

Clemens, J. D., Buick, I. S., & Stevens, G. (2016). Fluids, Melting, Granulites and Granites: A Controversy–Reply to the Commentary of. *Precambrian Research*, 278, 400-404.

Coggon, R., & Holland, T. J. B. (2002). Mixing properties of phengitic micas and revised garnet-phengite thermobarometers. *Journal of Metamorphic Geology*, 20, 683-696.

Connolly, J. A. D., & Cesare, B. (1993). C-O-H-S fluid composition and oxygen fugacity in graphitic metapelites. *Journal of metamorphic geology*, 11, 379-388.

Créon, L., Levresse, G., Remusat, L., Bureau, H., & Carrasco-Núñez, G. (2018). New method for initial composition determination of crystallized silicate melt inclusions. *Chemical Geology*, 483, 162-173.

Dubessy, J., Poty, B., & Ramboz, C. (1989). Advances in COHNS fluid geochemistry based on micro-Raman spectrometric analysis of fluid inclusions. *European Journal of Mineralogy*, 517-534.

Ewing, T. A., Hermann, J., & Rubatto, D. (2013). The robustness of the Zr-in-rutile and Ti-in-zircon thermometers during high-temperature metamorphism (Ivrea-Verbano Zone, northern Italy). *Contributions to Mineralogy and Petrology*, 165, 757-779.

Ferrero, S., Braga, R., Berkesi, M., Cesare, B., & Laridhi Ouazaa, N. (2014). Production of metaluminous melt during fluid-present anatexis: an example from the Maghrebian basement, La Galite Archipelago, central Mediterranean. *Journal of Metamorphic Geology*, 32, 209-225.

Ferrero, S., Wunder, B., Walczak, K., O'Brien, P. J., & Ziemann, M. A. (2015). Preserved near ultrahigh-pressure melt from continental crust subducted to mantle depths. *Geology*, *43*(5), 447-450.

Ferrero, S., Ziemann, M. A., Angel, R. J., O'Brien, P. J., & Wunder, B. (2016a). Kumdykolite, kokchetavite, and cristobalite crystallized in nanogranites from felsic granulites, Orlica-Snieznik Dome (Bohemian Massif): not evidence for ultrahigh-pressure conditions. *Contributions to Mineralogy and Petrology*, 171, 3.

Ferrero, S., Wunder, B., Ziemann, M. A., Wälle, M., & O'Brien, P. J. (2016b). Carbonatitic and granitic melts produced under conditions of primary immiscibility during anatexis in the lower crust. *Earth and Planetary Science Letters*, 454, 121-131.

Ferrero, F., & Angel, R. (2018). Micropetrology: are inclusions grains of truth?. *Journal of Petrology*, egy075, https://doi.org/10.1093/petrology/egy075 (in press).

Frost, B. R., & Frost, C. D. (2008). A geochemical classification for feldspathic igneous rocks. *Journal of Petrology*, 49, 1955-1969.

Gao, P., Zheng, Y. F., & Zhao, Z. F. (2016). Experimental melts from crustal rocks: a lithochemical constraint on granite petrogenesis. *Lithos*, 266, 133-157.

Garcia-Arias, M. (2018). Decoupled Ca and Fe + Mg content of S-type granites: An investigation on the factors that control the Ca budget of S-type granites. *Lithos*, https://doi.org/10.1016/j.lithos.2018.08.004 (in press).

Henk, A., Franz, L., Teufel, S., & Oncken, O. (1997). Magmatic underplating, extension, and crustal reequilibration: insights from a cross-section through the Ivrea Zone and Strona-Ceneri Zone, Northern Italy. *The Journal of Geology*, 105, 367-378.

Holland, T. J. B., & Powell, R. T. J. B. (1998). An internally consistent thermodynamic data set for phases of petrological interest. *Journal of Metamorphic Geology*, 16, 309-343.

Holland, T. J. B., & Powell, R. (2011). An improved and extended internally consistent thermodynamic dataset for phases of petrological interest, involving a new equation of state for solids. *Journal of Metamorphic Geology*, 29, 333-383.

Holtz, F., Johannes, W., Tamic, N., & Behrens, H. (2001). Maximum and minimum water contents of granitic melts generated in the crust: a reevaluation and implications. *Lithos*, 56, 1-14.

Huizenga, J. M., & Touret, J. L. (2012). Granulites, CO_2 and graphite. *Gondwana Research*, 22, 799-809.

Jackson, D. H., Mattey, D. P., & Harris, N. B. W. (1988). Carbon isotope compositions of fluid inclusions in charnockites from southern India. *Nature*, 333, 167.

Johannes, W., & Holtz F. (1996). Petrogenesis and experimental petrology of granitic rocks. Springer-Verlag, Berlin Heidelberg.

Kunz, B. E., Regis, D., & Engi, M. (2018a). Zircon ages in granulite facies rocks: decoupling from geochemistry above 850° C?. *Contributions to Mineralogy and Petrology*, 173, 26.

Kunz, B. E., Manzotti, P., von Niederhäusern, B., Engi, M., Darling, J. R., Giuntoli, F., & Lanari, P. (2018b). Permian high-temperature metamorphism in the Western Alps (NW Italy). *International Journal of Earth Sciences*, 107, 203-229.

Kleinefeld, B., & Bakker, R. J. (2002). Fluid inclusions as microchemical systems: evidence and modelling of fluid-host interactions in plagioclase. *Journal of Metamorphic Geology*, 20, 845-858.

Lamb, W. M., Valley, J. W., & Brown, P. E. (1987). Post-metamorphic CO_2-rich fluid inclusions in granulites. Contributions to Mineralogy and Petrology, 96(4), 485-495.

Lowenstern, J. B. (1995). Applications of silicate-melt inclusions to the study of magmatic volatiles. *Magmas, fluids, and ore deposits*, 23, 71-99.

Luth, W. C., Jahns, R. H. & Tuttle, O. F., (1964). The granite system at pressures of 4 to 10 kilobars. *Journal of Geophysical Research*, 69, 759-773.

Luvizotto, G. L., & Zack, T. (2009). Nb and Zr behavior in rutile during high-grade metamorphism and retrogression: an example from the Ivrea–Verbano Zone. *Chemical Geology*, 261, 303-317.

Milord, I., Sawyer, E. W., & Brown, M. (2001). Formation of diatexite migmatite and granite magma during anatexis of semi-pelitic metasedimentary rocks: an example from St. Malo, France. *Journal of Petrology*, 42, 487-505.

Montel, J. M., & Vielzeuf, D. (1997). Partial melting of metagreywackes, Part II. Compositions of minerals and melts. *Contributions to Mineralogy and Petrology*, 128, 176-196.

Morgan, G. B., & London, D. (2005). Effect of current density on the electron microprobe analysis of alkali aluminosilicate glasses. *American Mineralogist*, 90, 1131-1138.

Newton, R. C., Charlu, T. V., & Kleppa, O. J. (1980). Thermochemistry of the high structural state plagioclases. *Geochimica et Cosmochimica Acta*, 44, 933-941.

O'Connor, J.T. (1965). A classification for quartz-rich igneous rocks based on feldspar ratios. United States Geological Survey Professional Paper, 525, 79-84.

Palin, R. M., White, R. W., Green, E. C., Diener, J. F., Powell, R., & Holland, T. J. (2016). High-grade metamorphism and partial melting of basic and intermediate rocks. *Journal of Metamorphic Geology*, 34, 871-892.

Patiño Douce, A. E., & Harris, N. (1998). Experimental constraints on Himalayan anatexis. *Journal of Petrology*, 39, 689-710.

Peressini, G., Quick, J.E., Sinigoi, S., Hofmann, A.W., & Fanning, M. (2007). Duration of a large mafic intrusion and heat transfer in the lower crust: a SHRIMP U–Pb zircon study in the Ivrea-Verbano–Verbano Zone (Western Alps, Italy). *Journal of Petrology*, 48, 1185–1218.

Quick, J. E., Sinigoi, S., Snoke, A. W., Kalakay, T. J., Mayer, A., & Peressini, G. (2003). Geologic map of the southern Ivrea-Verbano Zone, northwestern Italy. *US Geological Survey*.

Redler, C., Johnson, T. E., White, R. W., & Kunz, B. E. (2012). Phase equilibrium constraints on a deep crustal metamorphic field gradient: metapelitic rocks from the Ivrea Zone (NW Italy). *Journal of Metamorphic Geology*, 30, 235-254.

Redler, C., White, R. W. & Johnson, T. E. (2013). Migmatites in the Ivrea Zone (NW Italy): Constraints on partial melting and melt loss in metasedimentary rocks from Val Strona di Omegna. *Lithos*, 175, 40-53.

Roedder, E., 1979. Fluid Inclusions as Samples of Ore Fluids. In: Barnes, H.L. (Ed.), Geochemistry of Hydrothermal Ore Deposits, 2nd ed. Wiley, New York, pp. 684–737.

Santosh, M., & Omori, S. (2008). CO2 flushing: a plate tectonic perspective. *Gondwana Research*, 13, 86-102.

Sawyer, E. W. (1987). The role of partial melting and fractional crystallization in determining discordant migmatite leucosome compositions. *Journal of Petrology*, 28, 445-473.

Sawyer, E. W., Dombrowski, C., & Collins, W. J. (1999). Movement of melt during synchronous regional deformation and granulite-facies anatexis, an example from the Wuluma Hills, central Australia. *Geological Society, London, Special Publications*, 168, 221-237.

Sawyer, E. W., Cesare, B., & Brown, M. (2011). When the continental crust melts. *Elements*, 7, 229-234.

Sawyer, E. W. (2014). The inception and growth of leucosomes: microstructure at the start of melt segregation in migmatites. *Journal of Metamorphic Geology*, *32*, 695-712.

Schmid, R. & Wood, B. J. (1976). Phase relationships in granulitic metapelites from the Ivrea-Verbano zone (Northern Italy). *Contributions to Mineralogy and Petrology*, 54, 255-279.

Schmid, S. M. (1993). Ivrea zone and adjacent southern Alpine basement. In: *Pre-Mesozoic Geology in the Alps* (eds. Raumer, J.F. & Neubauer, F.), pp. 567-583. Springer Verlag, Berlin.

Schnetger, B. (1994). Partial melting during the evolution of the amphibolite-to granulite-facies gneisses of the Ivrea Zone, northern Italy. *Chemical Geology*, 113, 71-101.

Sighinolfi, G. P., & Gorgoni, C. (1978). Chemical evolution of high-grade metamorphic rocks—anatexis and remotion of material from granulite terrains. *Chemical Geology*, 22, 157-176.

Sinigoi, S., Quick, J. E., Demarchi, G., & Klötzli, U. (2011). The role of crustal fertility in the generation of large silicic magmatic systems triggered by intrusion of mantle magma in the deep crust. *Contributions to Mineralogy and Petrology*, 162, 691-707.

Stevens, G., Villaros, A., & Moyen, J. F. (2007). Selective peritectic garnet entrainment as the origin of geochemical diversity in S-type granites. *Geology*, 35, 9-12.

Stevens, G., & Clemens, J. D. (1993). Fluid-absent melting and the roles of fluids in the lithosphere: a slanted summary?. *Chemical Geology*, 108, 1-17.

Tacchetto, T., Bartoli, O., Cesare, B., Berkesi, M., Aradi, L. E., Dumond, G., & Szabó, C. (2018). Multiphase inclusions in peritectic garnet from granulites of the Athabasca granulite terrane (Canada): Evidence of carbon recycling during Neoarchean crustal melting. *Chemical Geology*, https://doi.org/10.1016/j.chemgeo.2018.05.043 (in press).

Tajčmanová, L., Connolly, J. A. D., & Cesare, B. (2009). A thermodynamic model for titanium and ferric iron solution in biotite. *Journal of Metamorphic Geology*, 27, 153-165.

Tamic, N., Behrens, H., & Holtz, F. (2001). The solubility of H2O and CO2 in rhyolitic melts in equilibrium with a mixed CO2–H2O fluid phase. *Chemical geology*, 174, 333-347.

Taylor, J., & Stevens, G. (2010). Selective entrainment of peritectic garnet into S-type granitic magmas: Evidence from Archaean mid-crustal anatectites. *Lithos*, 120, 277-292.

Taylor, J., Nicoli, G., Stevens, G., Frei, D., & Moyen, J. F. (2014). The processes that control leucosome compositions in metasedimentary granulites: perspectives from the Southern Marginal Zone migmatites, Limpopo Belt, South Africa. *Journal of Metamorphic Geology*, 32, 713-742.

Thomen, A., Robert, F., Remusat, L., 2014. Determination of the nitrogen abundance in organic materials by NanoSIMS quantitative imaging. J. Anal. At. Spectrom. 29, 512-519.

Thompson, J. B., & Hovis, G. L. (1979). Entropy of mixing in sanidine.

Thompson, A. B., & Tracy, R. J. (1979). Model systems for anatexis of pelitic rocks. *Contributions to Mineralogy and Petrology*, 70, 429-438.

Touret, J. (1971). Le facies granulite en Norvege Meridionale: II. Les inclusions fluides. *Lithos*, 4, 423-436.

Touret, J. L. (1992). CO2 transfer between the upper mantle and the atmosphere: temporary storage in the lower continental crust. *Terra Nova*, 4, 87-98.

Santosh, M., & Omori, S. (2008). CO2 flushing: a plate tectonic perspective. *Gondwana Research*, 13, 86-102.

Vavra, G., Schmid, R., & Gebauer, D. (1999). Internal morphology, habit and U-Th-Pb microanalysis of amphibolite-to-granulite facies zircons: geochronology of the Ivrea Zone (Southern Alps). *Contributions to Mineralogy and Petrology*, 134, 380-404.

Vielzeuf, D., Clemens, J. D., Pin, C., Moinet, E. (1990). Granites, granulites, and crustal differentiation. In: Vielzeuf, D., Vidal, P. (Eds.), Granulites and Crustal Evolution. Nato ASI Series C-311. Kluwer, Dordrecht, pp. 59-85.

Wang, X., Chou, I. M., Hu, W., Burruss, R. C., Sun, Q., & Song, Y. (2011). Raman spectroscopic measurements of CO2 density: Experimental calibration with high-pressure optical cell (HPOC) and fused silica capillary capsule (FSCC) with application to fluid inclusion observations. *Geochimica et Cosmochimica Acta*, 75, 4080-4093.

Watson, E. B., & Brenan, J. M. (1987). Fluids in the lithosphere, 1. Experimentally-determined wetting. Earth and Planetary Science Letters, 85, 497-515.

Weinberg, R. F., & Hasalová, P. (2015a). Water-fluxed melting of the continental crust: A review. *Lithos*, 212, 158-188.

Weinberg, R. F., & Hasalová, P. (2015b). Reply to comment by JD Clemens and G. Stevens on “Water-fluxed melting of the continental crust: A review.”. *Lithos*, 234, 102-103.

White, R. W., & Powell, R. (2002). Melt loss and the preservation of granulite facies mineral assemblages. *Journal of Metamorphic Geology*, 20, 621-632.

White, R. W., Powell, R., & Holland, T. J. B. (2007). Progress relating to calculation of partial melting equilibria for metapelites. *Journal of Metamorphic Geology*, 25, 511-527.

White, R. W., & Powell, R. (2010). Retrograde melt–residue interaction and the formation of near-anhydrous leucosomes in migmatites. *Journal of Metamorphic Geology*, 28, 579-597.

Yakymchuk, C. (2017). Behaviour of apatite during partial melting of metapelites and consequences for prograde suprasolidus monazite growth. *Lithos*, 274, 412-426.

Zingg, A. (1980). Regional metamorphism in the Ivrea Zone (Southern Alps, N-Italy): field and microscopic investigations. *Schweizerische Mineralogische und Petrographische Mitteilungen*, 60, 153-179.

Caption for figures

Fig. 1: a) Geological map of the Ivrea Zone (modified after Redler et al., 2012). Legent: 1- Gneisses and schists; 2- Permian granites; 3- Kinzigite Formation; 4- Mafic rocks; 5- Ultramafic rocks; 6- Austroalpine and Penninic units; 7- Mineral isograds; 8- Faults; IL= Insubric Line; CMBL= Cossato-Mergozzo-Brissago Line; PL= Pogallo Line. b) Schematic section of Val di Strona di Omegna including the mineral isograds, as well as peak P-T conditions calculated by Redler et al. (2012; black boxes), Henk et al. (1997; white boxes) and Bea & Montero (1999; grey box). The values inside the boxes are temperature (top) in °C and pressure (bottom) in kbar. Stars represent the samples from this study. c) Extension of metamorphic zones as described in Redler et al. (2012). d) Extension of metamorphic zones as described by Schmid (1993). A = amphibolite facies; T = transition zone; G = granulite facies.

Fig. 2: Field aspects of the studied migmatites in the three zones. a) Fine-grained metatexite from upper amphibolite facies with narrow leucosomes as patches and along the foliation. b) Stromatic metatexite from the transition zone with cm-sized leucosomes and foliated melanosome enriched in

biotite and garnet. c) Close-up of a foliated residual diatexite from granulite facies with abundant garnet and sillimanite.

Fig. 3: Photomicrographs of the studied samples. a) Melanosome of metatexite (from upper amphibolite facies) composed of small garnet (Grt) porphyroblast, biotite (Bt), fibrolite (Fib), quartz (Qz) and relic prograde muscovite (Ms). b) Cluster of nanogranitoid and fluid inclusions under plane-polarized light c) Same under cross polarized light, showing the high birefringence of the fluid inclusions with carbonate. d) Typical microstructure of sample from the transition zone with garnet crystals surrounded by abundant biotite, fibrolitic to prismatic sillimanite and graphite. Note the presence of abundant inclusions in the cores of the garnet. e) Resorbed biotite, quartz and sillimanite associated to films of K-feldspar (grey arrows). f) Close-up of cluster of primary nanogranitoid (white arrow) and fluid (black arrow) inclusions in garnet core from the transition zone. g) Melanosome of residual diatexite from granulite facies composed of abundant prismatic sillimanite, garnet and some biotite.

Fig. 4: FESEM backscattered images from nanogranitoid inclusions.

Fig. 5: Representative Raman spectra of phases in: a to c) nanogranitoid inclusions. d) mixed inclusions. e and f) fluid inclusions.

Fig. 6: a) and b) Photomicrographs of a fluid inclusion with negative crystal shape under transmitted and cross-polarized light, respectively. c) FESEM image of fluid inclusion with siderite, pyrophyllite and graphite, and at the bottom EDS map for of Al, Si, Fe and C. Arrow points to porosity originally filled with carbonic fluid.

Fig. 7: a) Raman spectrum of glass after re-melting experiment in (b). b) to j) BSE-SEM images of representative examples of nanogranitoid inclusions after piston cylinder experiments. b) Homogeneous glass from experiment at 850°C, 1 GPa and 20 h. c) Homogeneous glass from

experiment at 820°C, 1 GPa and 20 h. d) Homogeneous glass from experiment at 900°C, 1.2 GPa and 5 h. e) Inclusion with homogeneous glass and trapped graphite. f) Inclusion with homogeneous glass and trapped plagioclase. g) and h) Examples of inclusions with bubbles (white arrows). i) Partially melted nanogranitoid with corroded biotite (white arrow), quartz (yellow arrow) and glass (black arrow). j) Example of interaction between melt and host shown by the presence of new euhedral orthopyroxene crystals (white arrow) and irregular boundaries of the host with darker shade of grey (yellow arrow) in the BSE image. UA= upper amphibolite facies, T = transition zone, G= granulite facies.

Fig. 8: Harker diagrams of analyzed MI from Ivrea zone. Grey field represent leucosome compositions from Bea & Montero (1999). a) AI [molar Al_2O_3-(Na_2O+K_2O)] versus ASI [molar Al_2O_3/(CaO+Na_2O+K_2O)], fields after Frost & Frost (2008).

Fig. 9: CIPW normative diagrams. MI from the literature from Bartoli et al. (2016) and Acosta-Vigil et al. (2016). a) An-Or-Ab field after O'Connor (1965). b) Qz-Or-Ab showing cotectic lines at 5 and 10 kabar (Luth, Jahns, & Tuttle 1964).

Fig. 10: H_2O (wt.%) and CO_2 (ppm) contents of re-homogenized nanogranite inclusions. Symbols: circles= STR36; purple diamonds= STR28; white diamonds= IVT21; squares = STR22. UA = upper amphibolite facies; T = transition zone; G = granulite facies.

Fig. 11: P–T estimates for metapelites from Val Strona di Omegna. a) P–T phase diagram for a probable protolith composition obtained applying the melt-reintegration approach (see above and Figure S1). Isopleths of modal proportions of melt, biotite and garnet are reported. b) Summary diagram showing the P–T position of the liquid-in, muscovite-out and biotite-out curves reported in the literature for fertile metapelites from Val Strona di Omegna (data from Redler et al., 2012, 2013; Bartoli, 2018; this study). The grey field represents the inferred metamorphic field gradient (Redler et al., 2012).

Caption for Tables

Table 1: Representative analyses of garnet, biotite, muscovite, plagioclase and K-feldspar.

Table 2: Major element composition of re-homogenized melt inclusions.

Table 3: H_2O (wt.%) and CO_2 (ppm) concentrations measured in re-homogenized melt inclusions by NanoSIMS.

Caption for figures

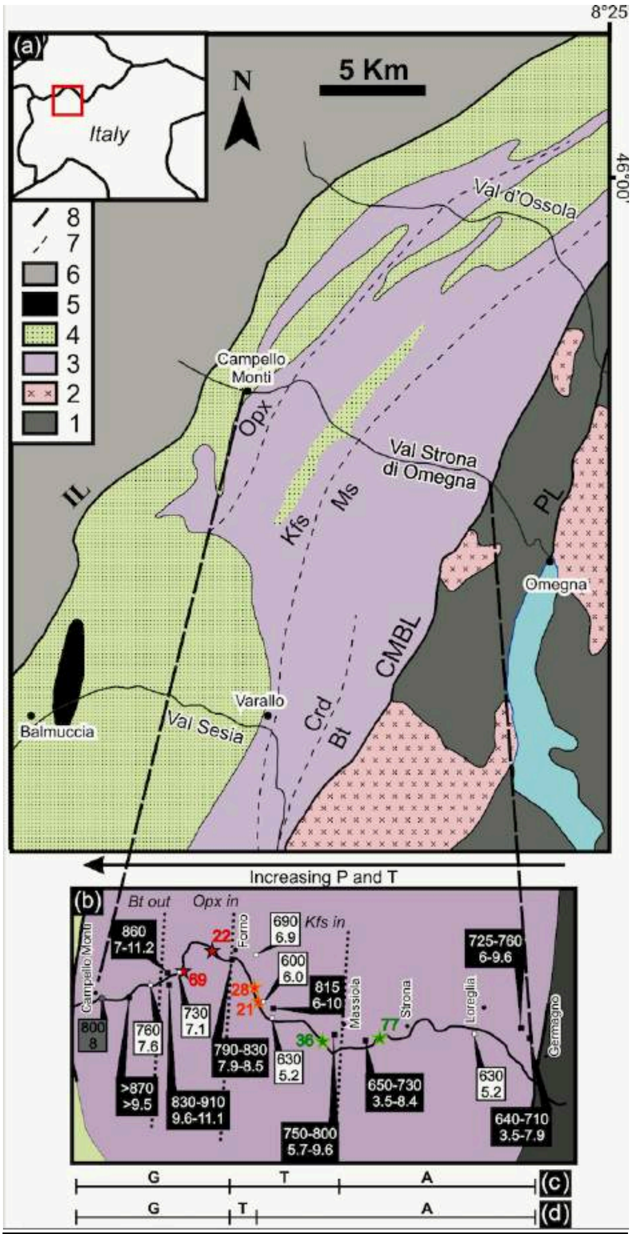

Fig. 1: a) Geological map of the Ivrea Zone (modified after Redler et al., 2012). Legent: 1- Gneisses and schists; 2- Permian granites; 3- Kinzigite Formation; 4- Mafic rocks; 5- Ultramafic rocks; 6- Austroalpine and Penninic units; 7- Mineral isograds; 8- Faults; IL= Insubric Line; CMBL= Cossato-Mergozzo-Brissago Line; PL= Pogallo Line. b) Schematic section of Val di Strona di Omegna including the mineral isograds, as well as peak P-T conditions calculated by Redler et al. (2012; black boxes), Henk et al. (1997; white boxes) and Bea & Montero (1999; grey box). The values inside the boxes are temperature (top) in °C and pressure (bottom) in kbar. Stars represent the samples from this study. c)

Extension of metamorphic zones as described in Redler et al. (2012). d) Extension of metamorphic zones as described by Schmid (1993). A = amphibolite facies; T = transition zone; G = granulite facies.

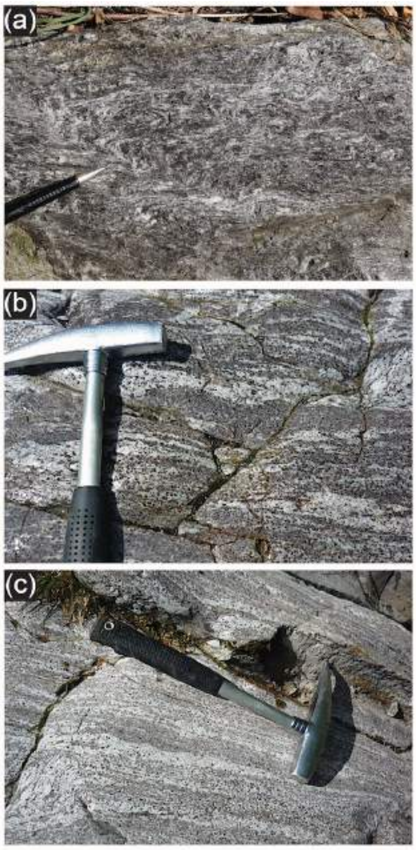

Fig. 2: Field aspects of the studied migmatites in the three zones. a) Fine-grained metatexite from upper amphibolite facies with narrow leucosomes as patches and along the foliation. b) Stromatic metatexite from the transition zone with cm-sized leucosomes and foliated melanosome enriched in biotite and garnet. c) Close-up of a foliated residual diatexite from granulite facies with abundant garnet and sillimanite.

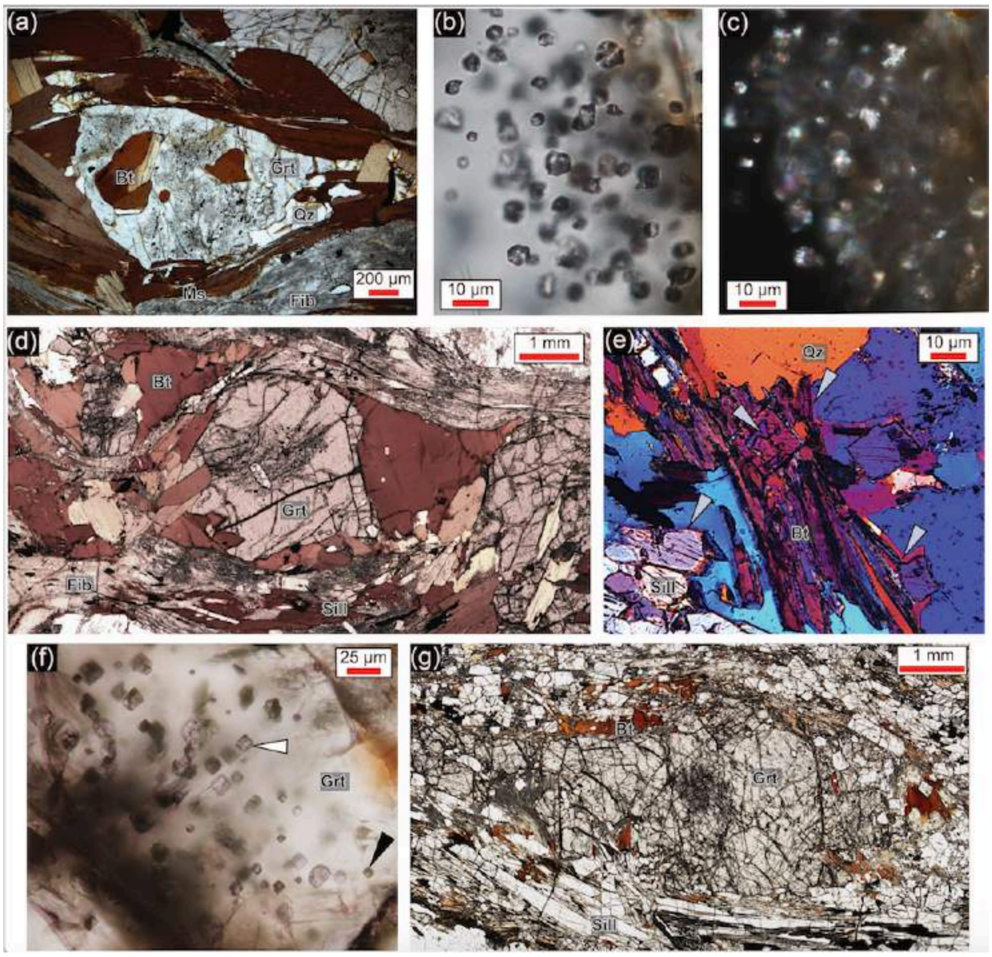

Fig. 3: Photomicrographs of the studied samples. a) Melanosome of metatexite (from upper amphibolite facies) composed of small garnet (Grt) porphyroblast, biotite (Bt), fibrolite (Fib), quartz (Qz) and relic prograde muscovite (Ms). b) Cluster of nanogranitoid and fluid inclusions under plane-polarized light c) Same under cross polarized light, showing the high birefringence of the fluid inclusions with carbonate. d) Typical microstructure of sample from the transition zone with garnet crystals surrounded by abundant biotite, fibrolitic to prismatic sillimanite and graphite. Note the presence of abundant inclusions in the cores of the garnet. e) Resorbed biotite, quartz and sillimanite associated to films of K-feldspar (grey arrows). f) Close-up of cluster of primary nanogranitoid (white arrow) and fluid (black arrow) inclusions in garnet core from the transition zone. g) Melanosome of residual diatexite from granulite facies composed of abundant prismatic sillimanite, garnet and some biotite.

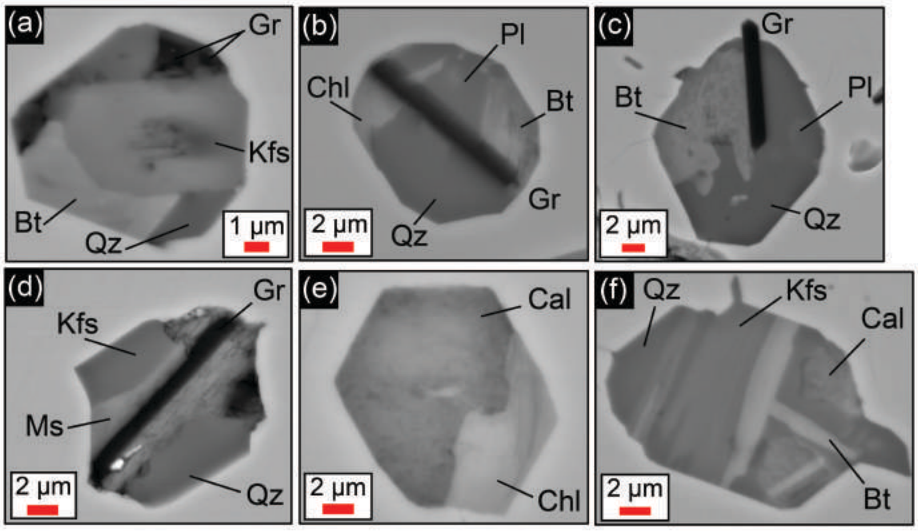

Fig. 4: FESEM backscattered images from nanogranitoid inclusions.

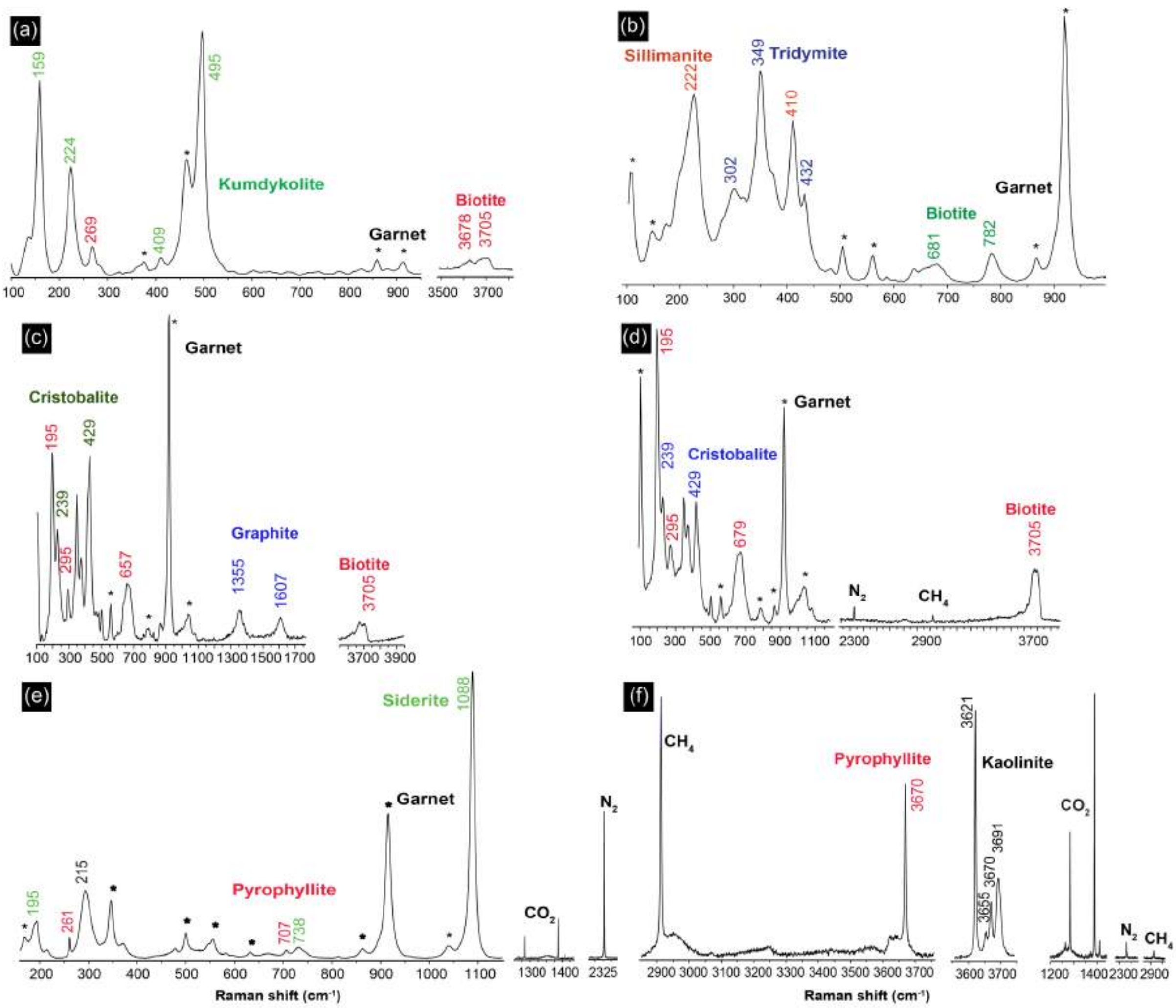

Fig. 5: Representative Raman spectra of phases in: a to c) nanogranitoid inclusions. d) mixed inclusions. e and f) fluid inclusions.

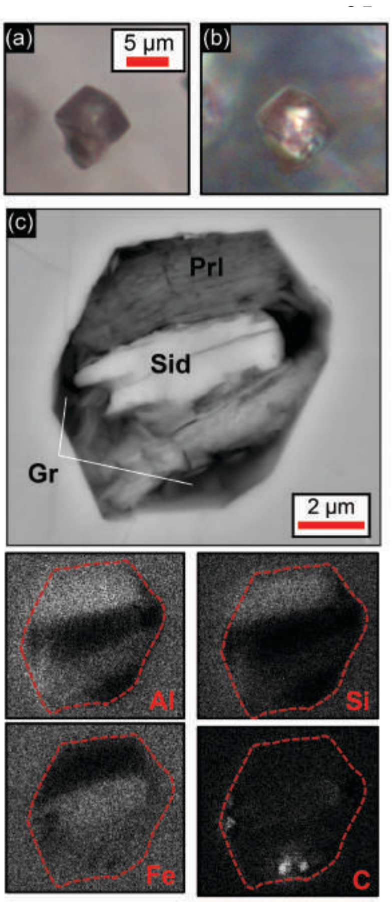

Fig. 6: a) and b) Photomicrographs of a fluid inclusion with negative crystal shape under transmitted and cross-polarized light, respectively. c) FESEM image of fluid inclusion with siderite, pyrophyllite and graphite, and at the bottom EDS map for of Al, Si, Fe and C. Arrow points to porosity originally filled with carbonic fluid.

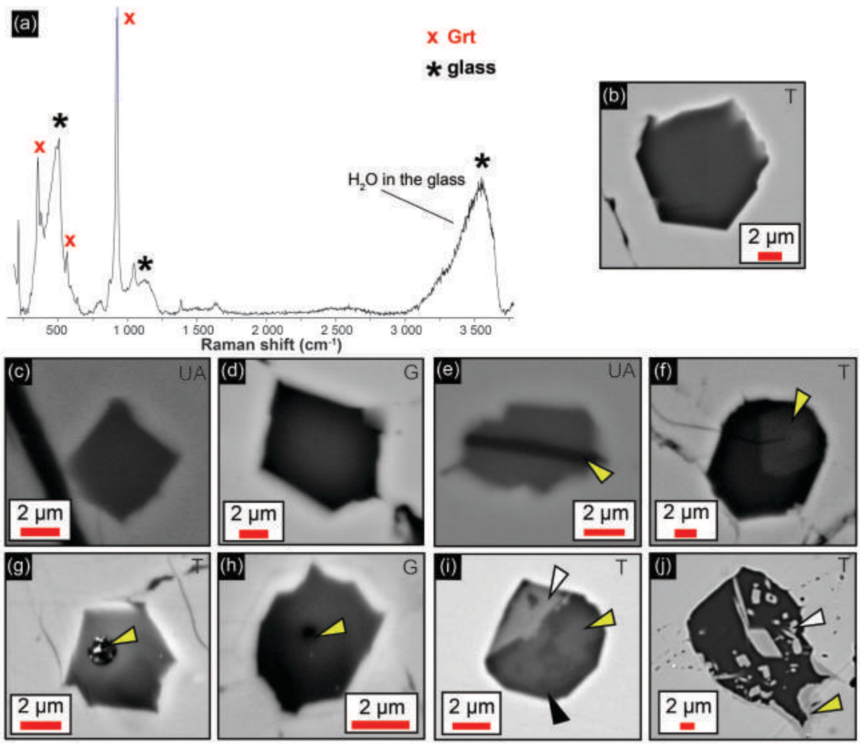

Fig. 7: a) Raman spectrum of glass after re-melting experiment in (b). b) to j) BSE-SEM images of representative examples of nanogranitoid inclusions after piston cylinder experiments. b) Homogeneous glass from experiment at 850°C, 1 GPa and 20 h. c) Homogeneous glass from experiment at 820°C, 1 GPa and 20 h. d) Homogeneous glass from experiment at 900°C, 1.2 GPa and 5 h. e) Inclusion with homogeneous glass and trapped graphite. f) Inclusion with homogeneous glass and trapped plagioclase. g) and h) Examples of inclusions with bubbles (white arrows). i) Partially melted nanogranitoid with corroded biotite (white arrow), quartz (yellow arrow) and glass (black arrow). j) Example of interaction between melt and host shown by the presence of new euhedral orthopyroxene crystals (white arrow) and irregular boundaries of the host with darker shade of grey (yellow arrow) in the BSE image. UA= upper amphibolite facies, T = transition zone, G= granulite facies.

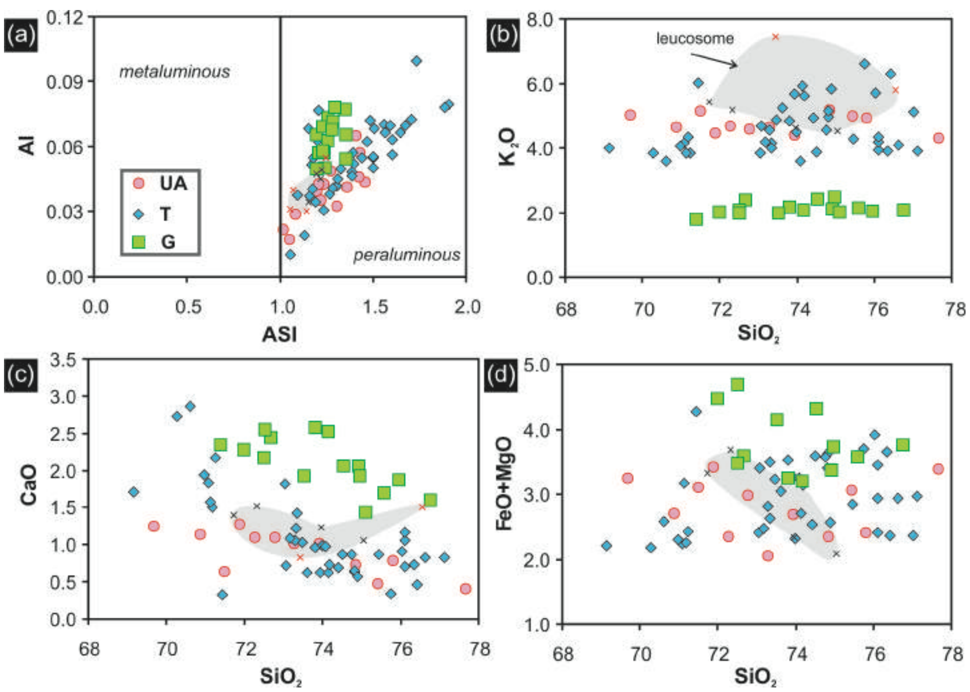

Fig. 8: Harker diagrams of analyzed MI from Ivrea zone. Grey field represent leucosome compositions from Bea & Montero (1999). a) AI [molar Al_2O_3-(Na_2O+K_2O)] versus ASI [molar Al_2O_3/(CaO+Na_2O+K_2O)], fields after Frost & Frost (2008).

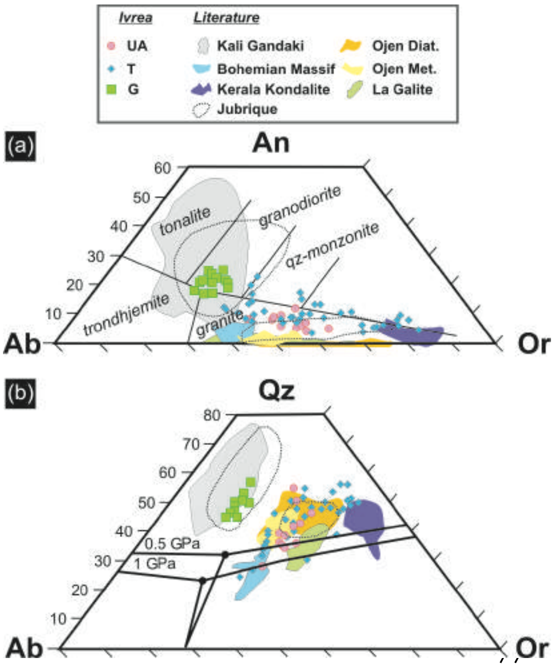

Fig. 9: CIPW normative diagrams. MI from the literature from Bartoli et al. (2016) and Acosta-Vigil et al. (2016). a) An-Or-Ab field after O'Connor (1965). b) Qz-Or-Ab showing cotectic lines at 5 and 10 kabar (Luth, Jahns, & Tuttle 1964).

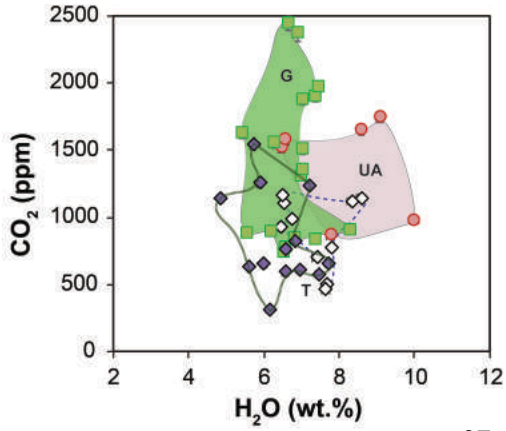

Fig. 10: H_2O (wt.%) and CO_2 (ppm) contents of re-homogenized nanogranite inclusions. Symbols: circles= STR36; purple diamonds= STR28; white diamonds= IVT21; squares = STR22. UA = upper amphibolite facies; T = transition zone; G = granulite facies.

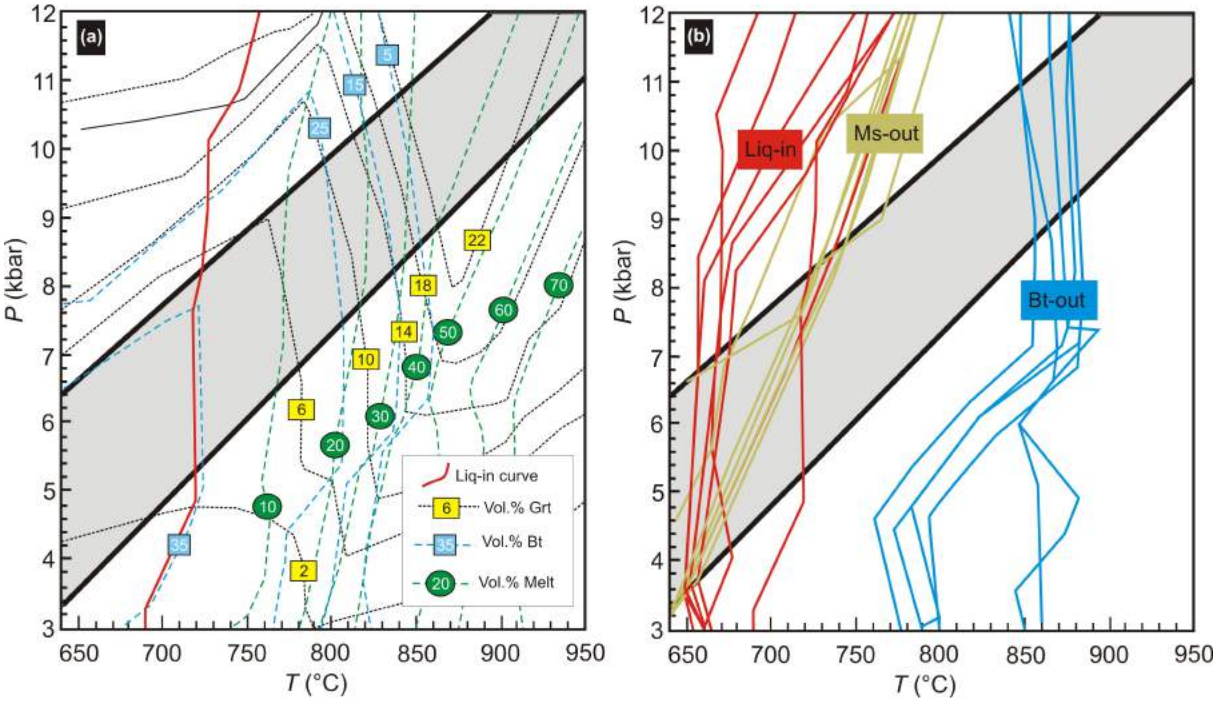

Fig. 11: P–T estimates for metapelites from Val Strona di Omegna. a) P–T phase diagram for a probable protolith composition obtained applying the melt-reintegration approach (see above and Figure S1). Isopleths of modal proportions of melt, biotite and garnet are reported. b) Summary diagram showing the P–T position of the liquid-in, muscovite-out and biotite-out curves reported in the literature for fertile metapelites from Val Strona di Omegna (data from Redler et al., 2012, 2013; Bartoli, 2018; this study). The grey field represents the inferred metamorphic field gradient (Redler et al., 2012).

Caption for Tables

Table 1: Representative analyses of garnet, biotite, muscovite, plagioclase and K-feldspar.

Table 2: Major element composition of re-homogenized melt inclusions.

Table 3: H_2O (wt.%) and CO_2 (ppm) concentrations measured in re-homogenized melt inclusions by NanoSIMS.